J. Fluid Mech. (1979), *vol.* 91, *part* 4, *pp.* 697–730
Printed in Great Britain

A vortex theory of animal flight. Part 1. The vortex wake of a hovering animal

By J. M. V. RAYNER

Department of Applied Mathematics and Theoretical Physics, University of Cambridge†

(Received 18 May 1978)

The distribution of vorticity in the wake of a hovering bird or insect is considered. The wake is modelled by a chain of coaxial small-cored circular vortex rings stacked one upon another; each member of the chain is generated by a single wing-stroke. Circulation is determined by the animal's weight and the time for which a single ring must provide lift; ring size is calculated from the circulation distribution on the animal's wing. The theory is equally applicable to birds and insects, although the mechanism of ring formation differs. This approach avoids the use of lift and drag coefficients and is not bound by the constraints of steady-state aerodynamics; it gives a wake configuration in agreement with experimental observations. The classical momentum jet approach has steady momentum flux in the wake, and is difficult to relate to the wing motions of a hovering bird or insect; the vortex wake can be related to the momentum jet, but adjacent vortex elements are disjoint and momentum flux is periodic.

The evolution of the wake starting from rest is considered by releasing vortex rings at appropriate time intervals and allowing them to interact in their own velocity fields. The resulting configuration depends on the feathering parameter f (which depends on the animal's morphology); f increases with body size. At the lower end of the wake rings coalesce to form a single large vortex, which breaks away from the rest of the wake at intervals. Wake contraction depends on f; the minimum areal contraction of one-half (as in momentum-jet theory) occurs only in the limit $f \to 0$, but values calculated for smaller insects of just over one-half suggest that the momentum jet may be a good approximation to the wake when f is small.

Induced power in hovering is calculated as the limit of the mean rate of increase of wake kinetic energy as time progresses. It can be related to the classical momentum-jet induced power by a simple conversion factor. For an insect or hummingbird the usual momentum-jet estimate may be between 10 and 15% too low, but for a bird it may be as much as 50% too low. This suggests that few, if any, birds are able to sustain aerobic hovering, and that as small a value of f as possible would be necessary if the bird were to hover.

Tip losses (energy cost of the vortex-ring wake compared with the equivalent momentum jet) are negligible for insects, but can be in the range 15–20% for birds.

† Present address: Department of Zoology, University of Bristol.

0022-1120/79/4170-6250 $02.00

1. Introduction

This paper describes a theory for the flight of a hovering animal based on the vorticity present in its wake. By the theory the flight characteristics, and in particular the rate of working, may be estimated. For reasons described below, the vortex model consists of a chain of horizontal vortex rings stacked one above another. The companion paper (Rayner 1979*a*, afterwards referred to as II) describes the application of the theory to forward avian flight.

A common approach to the problem of hovering flight (e.g. Hoff 1919; Hainsworth & Wolf 1972; Weis-Fogh 1972) is the actuator disk and its associated Rankine–Froude momentum jet, as used in propeller theory (Glauert 1935). This assumes that there is no vorticity present in the body of the wake, and that the wake has a well-defined boundary within which mass and momentum are conserved; effectively this boundary is a thin vortex sheet, although a cylindrical vortex sheet is unlikely to be stable. Other defects of the actuator-disk theory are the geometrical assumptions used in applying conservation laws, which become meaningless if the boundary distorts or breaks up, and the lack of consideration of the mechanism on the disk itself by which a pair of wings oscillating back and forth can generate a steady momentum jet.

In an effort to overcome the second problem a blade element theory has been widely applied in the study of propellers. It was tentatively applied to insect flight by Osborne (1951), and then with more success by Weis-Fogh (1972, 1973). This theory assumes that each element of the wing operates under steady-state aerofoil conditions, the lift δL generated by the section being given by an equation of the form

$$\delta L = \tfrac{1}{2}\rho \delta S C_L u^2, \tag{1}$$

where ρ is the air density, δS the element's area, u its velocity through the air, and C_L the lift coefficient; C_L depends on the cross-section and angle of attack of the element, but is largely independent of u, except in so far as the cross-section and angle of attack themselves vary with velocity.

Most existing flight studies (Pennycuick 1968; Weis-Fogh 1972, 1973; Norberg 1975, 1976) use a blade element theory combined with the induced fluid velocities predicted by the momentum jet. These all require knowledge of the lift and drag coefficients and the assumption that steady state aerodynamics pertains. In this vortex theory we need not make such a sweeping assumption, and do not need values for the lift and drag coefficients.

The maximum lift obtainable from an aerofoil is limited by the separation of the upper surface boundary layer; for a simple rigid non-permeable wing the maximum lift coefficient obtainable is about 1, but the use of lift-enhancing devices such as leading-edge slots and through-wing suction can raise the maximum to about 3. The few indications available suggest that very large lift coefficients are required by hovering animals. Basing calculations on careful observations, Weis-Fogh (1972) found that an average C_L of 1·8 was required by the hummingbird *Amazilia*, near to the maximum. More puzzlingly, Norberg (1975) found that the pied flycatcher *Ficedula hypoleuca* required $C_L = 5{\cdot}3$ to hover, apparently in still air. Unless remarkable high lift devices are at an animal's disposal, steady-state aerodynamics cannot give a complete description of hovering and slow speed flight in insects and smaller

birds. Some larger birds, for example pigeons, can hover for a few strokes, which suggests that they have sufficient aerodynamic capacity and structural strength, but insufficient power, for prolonged aerobic hovering; it is reasonable to expect that power consumption determines the maximum size above which animals cannot hover, either continuously or for short periods. It is not clear from Norberg's paper whether the flycatcher concerned was capable of sustained hovering. As it was hovering before landing on a nest it seems most likely that the muscles were becoming anaerobic, and that the animal would not have been capable of continuous hovering. There is no reliable evidence that any bird (except for the rather unusual hummingbird) is able to hover continuously. Observations of such birds as the kestrel hovering can be explained by slow flight into a wind, so that they merely appear stationary.

Equation (1) may still apply to animal hovering, but its use should be cautious because of the lack of information on the behaviour of C_L under unsteady high lift conditions. Any theory which avoids the use of lift and drag coefficients for the wing sections will be less dependent on the steady-state assumptions, and will be more appropriate to the study of animal flight. We consider the topic of lift coefficients in greater detail in II, § 5.

A wing starting from rest cannot build up its full circulation immediately, but is subject to a time delay (the Wagner effect); equally, as the wing slows there is a certain amount of hysteresis as the circulation is not shed into the wake as rapidly as the steady-state theory suggests. It seems likely that the combined effects of these two phenomena would be to reduce the average lift coefficient for an oscillating wing slightly; no such mechanism is known by which a lift coefficient as high as 5 might be obtained. Cone (1968) suggests that, if the wings could start sufficiently close to one another for the bound vortex of one to be the trailing vortex of the other, the animal might ease the Wagner effect and achieve a more rapid build-up of circulation. From careful observation of the chalcid wasp *Encarsia formosa*, Weis-Fogh showed that for these tiny ($\approx$ 1 mm) insects lift enhancement from the clap-and-fling does indeed take place (Weis-Fogh 1973; Lighthill 1973). The clap-and-fling motions allow a sudden rush of air into the gap between the wings, so that circulation is set up almost instantaneously, thus allowing some increase of lift. Variations on the clap-and-fling have been observed in many orders of insects and birds, but despite the importance of the mechanism it is unlikely to explain Norberg's high lift coefficient for the flycatcher; in the measurements concerned the wing tips remained at least 70° apart throughout, although the secondary feathers may have touched.

It is not possible to give a detailed discussion of the lift coefficient required in hovering flight or of the mechanisms by which they are obtained. This problem remains one of the main stumbling blocks in any theory of animal flight. Many insects have pairs of wings whose interaction is ill understood, and the wings of some species consist of little more than feather-like plumes. Bird wings are of course very complicated, with many refinements presumably intended to assist lift generation and drag reduction; the emarginated and separated primary feathers and the alula (a form of leading-edge slot) can all assist (Nachtigall & Kempf 1971; Oehme & Kitzler 1975*a*), but we can do little more than speculate on how, and to what effect. For the purposes of this discussion it is sufficient to recall that generally the animals concerned can hover, so that in most cases there must be some form of lift enhancement in operation.

We shall deduce results from a study of the vorticity present in the animal's wake,

rather than from the more usual approach of wing aerodynamics. The true distribution of vorticity in the wake is highly complex, and for an effective investigation it needs careful simplification. Consideration of the wake of a flying aircraft has proved very instructive (von Kármán & Burgers 1935) and our calculations are analogous to these classical results. Hovering is defined as the mode of flight in which the body is at rest relative to undisturbed air, with the wake vertically beneath the animal, and with all fluid motions induced by the beating wings. The wing disk is the approximately circular area mapped out by the leading edges of the wings as they oscillate back and forth; it is assumed to be planar and tilted such that the resulting wake momentum is vertical (see below, and §3).

The aircraft wake consists of a vortex sheet shed from the trailing edges of the wings, which in time rolls up into two parallel straight line vortices which drift downwards under their mutual interaction. The separation and core radius of the resulting vortex pair are determined by the distribution of wing circulation, and may be found under certain simplifying assumptions. The optimum circulation distribution in terms of power saving is elliptic loading, with constant downwash; in this case the separation is 0·785 times the wing-span, and the core radius 0·171 times.

In a flapping animal the situation is more complex. While the wings produce lift there must be some form of trailing vortex sheet, containing elements of transverse or cross-stream vorticity if the wing velocity and circulation vary during the stroke. In most birds the upstroke is feathered and no vorticity is shed, so the downstroke will leave discrete elements of vorticity at intervals along the wake. When the bird is hovering these vortex elements lie one above another, drifting downwards under their self-induced velocity and their mutual interaction. A similar, although differently scaled, wake pattern describes the wake of a hovering insect; vortex elements are generated by both parts of the wing-stroke, and as we see in §3, may also be assumed to be discrete.

Each vortex element will initially be a vortex sheet of varying local strength lying along the trajectory of the wings. By analogy with the aircraft wake, this rolls up into a loop of concentrated vorticity; we must assume that this roll-up occurs reasonably quickly, and does not admit any destructive instability. The strength of this vortex loop must be the same as the total circulation shed from the wing into the portion of the sheet which composes it; its impulse and energy will be the same as those of the sheet provided that roll-up occurs rapidly. These conditions enable the size of the loop to be determined if its shape is known. If the wings beat through a complete arc the vortex sheet will be circular in plan, and it is clear that the concentrated vortex will be a circular ring. For smaller wing-beats we can see no alternative to assuming that the vortex loop is also circular. The circular vortex ring is the only shape of vortex loop which travels under its self-influence without deforming; its velocity and self-energy are well known. This assumption of circular vortex rings provides the only wake configuration which is simple enough (thanks to the azimuthal symmetry) to allow relatively simple calculations of the velocity field and kinetic energy of a number of rings, and which therefore allows us to trace the evolution of the wake.

It is interesting to discuss the relation between the kinematics of the animal's wing-stroke and the resulting vortex distribution. The sense of the vorticity is such that it will be convected downwards, and its impulse can support the animal's weight.

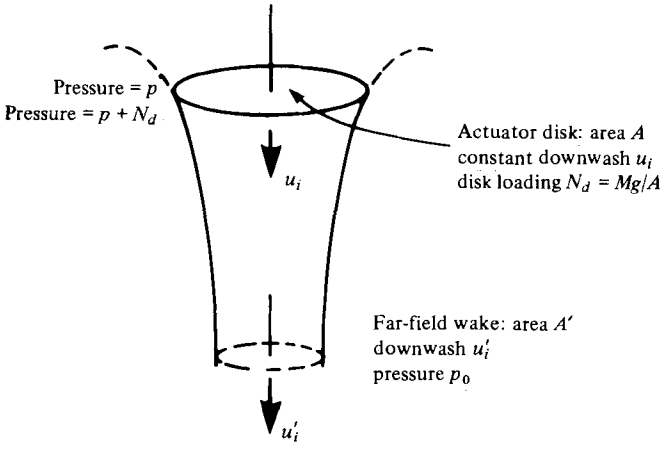

FIGURE 1. Diagram of actuator disk and momentum jet.

The vorticity is not generated instantaneously, but rather throughout the stroke. Because of the downward convection of vorticity caused by the induced fluid downwash through the wing disk the oldest portions of vorticity must have been generated at a higher point than the latest portions; the stroke plane must be inclined to the horizontal if the net impulse generated in a stroke is vertical. We see in § 8 how the inclination of the stroke plane may be estimated. The other important kinematic parameter is the stroke amplitude. Reducing the amplitude will result in a vortex sheet of smaller area, so to obtain the same impulse the circulation must be greater, and hence the lift coefficient needed is greater. Different vortex-ring radii are also achieved by varying the wing circulation distribution (as far as an individual bird or insect is able); larger ring radii will be shown to result in both lower induced power and lower lift coefficient. The increase in wake energy associated with any circulation increase (despite the increased spacing between elements which would result) is likely to encourage any animal to use as large an amplitude as possible within the limits of its structure. A large amplitude also permits possible benefit from the clap-and-fling mechanism.

We assume that the wake is formed entirely of circular rings arranged coaxially on top of each other, and then calculate the shape of the wake and the rate of working required to generate it. We have seen above how this concept of the wake corresponds to what we might expect from the wing motions; the use of circular vortex rings makes the problem reasonably tractable.

2. The actuator disk and momentum jet theory

Consideration of the actuator disk and its associated momentum jet indicates the general nature of the flow field and provides a convenient yardstick for comparison with the results of the vortex theory. We give a brief outline of the theory here.

A diagram of the disk and its wake, with the notation used, is given in figure 1. The flow field contains momentum flux sufficient to support an animal of weight Mg with its centre of gravity at the centre of the disk. In the simplest application we assume that vertical force and downwash are constant across the disk and that there

is no azimuthal flow; it is possible to extend the theory to include both varying downwash and rotational flow but the induced power is minimized when these are absent; Ellington (1978) has shown that the minimum is shallow. We use the ideal case of minimum induced power for comparison with the vortex wake. The induced power is the rate of working required to generate the induced momentum jet; it is the same as the rate of working by the wings in overcoming induced drag, but by calculating it in this way we avoid the need to know lift and induced drag coefficients for the wings. It is not the only component of the animal's power consumption, since work is also done against the profile drag (form plus frictional drag) of the wings, and in accelerating the wings during the stroke.

All fluid crossing the disk receives a pressure increment such that the vertical force supporting the animal is distributed evenly across the disk. The presesure difference between the two sides of the disk is equal to the disk loading N_d; the reaction of the wake momentum must be able to support the animal and therefore the induced velocities are determined. We also assume that the system is time independent, and that mass and momentum are conserved in the body of the wake. With ambient pressure p_0 and pressure just above the disk p, we apply Bernoulli's principle to a streamline passing through the disk. Above the disk

$$p_0 = p + \tfrac{1}{2}\rho u_i^2, \tag{2}$$

while beneath the disk

$$p + N_d + \tfrac{1}{2}\rho u_i^2 = p_0 + \tfrac{1}{2}\rho u_i'^2. \tag{3}$$

The downwash through the disk, u_i, is constant across the disk. From (2) and (3) the induced velocity u_i' in the far field is given by

$$u_i' = (2N_d/\rho)^{\frac{1}{2}}. \tag{4}$$

From mass conservation within the boundary of the wake

$$\rho A u_i = \rho \lambda A u_i', \tag{5}$$

where A is the disk area and λ the areal contraction, and from the identity between rate of increase of momentum and weight supported

$$\rho A u_i u_i' = Mg, \tag{6}$$

or

$$u_i u_i' = N_d/\rho. \tag{7}$$

From (4) and (7) we deduce that

$$u_i = (N_d/2\rho)^{\frac{1}{2}}, \quad u_i' = 2u_i, \tag{8), (9}$$

while from (5) the contraction coefficient

$$\lambda = \tfrac{1}{2}. \tag{10}$$

The induced power $P_{i,M}$ is given by

$$P_{i,M} = Mgu_i = Mg(Mg/2\rho A)^{\frac{1}{2}}. \tag{11), (12}$$

The assumptions of momentum and mass conservation lead directly to the conclusion that the wake contracts in area by a factor of $\frac{1}{2}$.

In the wake the fluid downwash is constant across any cross-section, while outside the wake there is no flow; there is a discontinuity in the tangential velocity across the boundary of the wake equal in the far field to the induced velocity u_i' on the cross-

section. This flow is identical to that generated by a cylindrical vortex sheet of circulation u_i' per unit length. In such a vortex sheet the vorticity is convected down the tube at velocity $\frac{1}{2}u_i'$; maintaining the velocity discontinuity across the sheet, we see that the flow within must be a constant velocity of u_i', with no flow outside. An alternative description to the momentum jet would be the cylindrical vortex sheet.

The shape assumed by a semi-infinite cylindrical vortex sheet as it deforms under its own influence must be the same as the shape of the boundary of the momentum jet. It would be valuable to calculate this shape to find the dependence of the dimensions of the contraction neck on disk area and loading; as yet this problem has proved intractable.

The actuator disk gives an idealized description of the true state of affairs on an animal's wing disk. In fact, vorticity is not generated steadily but in discrete units associated with the wing-beats, and in addition there may be vorticity present within the body of the wake. We shall take account of the unsteadiness by decomposing the cylindrical vortex sheet into discrete circular vortex rings, each associated with a single wing-beat. Such a description of the wake is in good theoretical agreement with what we might expect, and accords well with the little experimental evidence available. Since flow through the boundary of the wake is possible, mass and momentum need not be conserved, and we can expect contraction coefficients λ greater than $\frac{1}{2}$; the coefficients will be shown to depend upon the disk loading and area and upon the kinematics of the wing-stroke.

3. Biological application

The data required to describe the flight of a hovering animal may be divided into two groups. First, the *morphologic* parameters describe the structural characteristics of the animal; those of most relevance are the body mass M and wing semi-span b. To estimate the power available from the muscles we also need the masses of the main flight muscles. The area A of the wing disk used in § 2 is equal to πb^2, so that the disk loading N_d is $Mg/\pi b^2$. The *kinematic* parameters describe the dynamics of the wing-beat; they include the stroke period T, downstroke ratio τ (proportion of stroke spent on downstroke), stroke-plane angle γ and stroke amplitude ϕ. See figure 2 for a diagram of the notation. Some sample morphologic data are shown in table 1. The stroke-plane angle γ depends on the animal involved, and is discussed in § 8; ϕ usually lies between $\frac{2}{3}\pi$ and π, and τ is about one-half (exactly $\frac{1}{2}$ for insects and hummingbirds: see below). Morphologic and kinematic data for insects are given by Weis-Fogh (1973). Morphologic data for birds may be found in Greenewalt (1962) and kinematic data in, for instance, Oehme & Kitzler (1974, 1975*b*). Background information on insect flight is discussed thoroughly by Nachtigall (1974; this book does not discuss the latest developments in unsteady flight mechanisms, for which see Weis-Fogh 1973). Rüppell (1977) gives a valuable general discussion of bird flight.

We find that the relevant parameters may be reduced to two. The first, the initial radius of each vortex ring, will be discussed in § 5, and is determined from the unsteady aerodynamics of the wings themselves. The second, the *feathering parameter* f, summarizes the relevant kinematic and morphologic data for the animal; f is non-dimensional, and allows a straightforward non-dimensionalization of the entire problem. Mks units are used throughout.

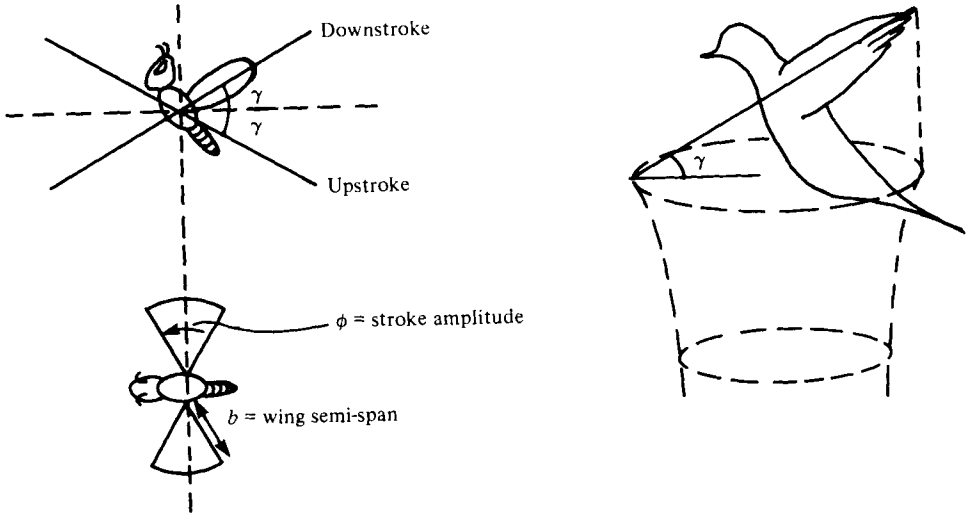

(*a*) (*b*)

FIGURE 2. Diagrammatic view of hovering animals. (*a*) Normal hovering; note that upstroke and downstroke are symmetrical. (*b*) Avian hovering, showing downstroke wing-tip path.

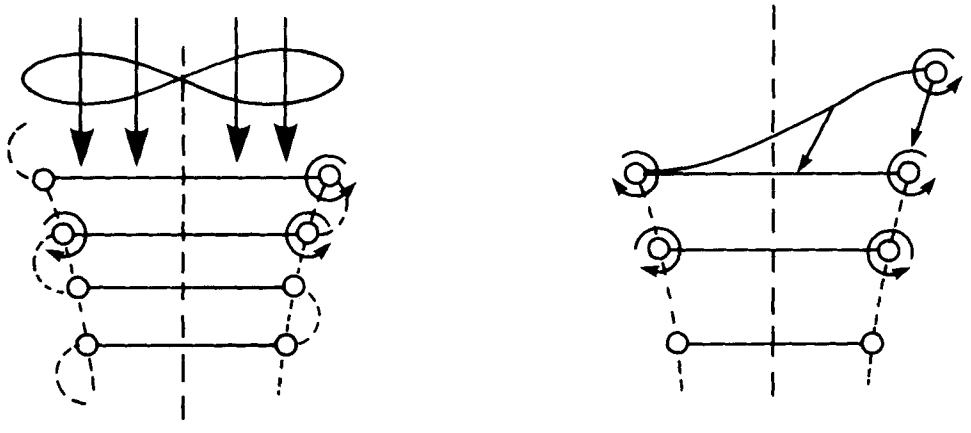

(*a*) (*b*)

FIGURE 3. Diagrams of wake formation mechanisms in (*a*) normal hovering and (*b*) avian hovering, showing a cross-section of the wake beneath the animal. The sense of vortex-ring circulation is indicated by curved arrows; vertical arrows indicate vorticity convection.

The feathering parameter f is defined as the square of ratio between the ideal velocity u_i [see (8)] on the wing disk and the *mean tip velocity* u_t. u_t is defined as the half-circumference of the wing disk divided by the time T_w for which a single vortex ring must support the animal, i.e.

$$u_t = \pi b / T_w. \tag{13}$$

The true tip velocity is given by the actual distance travelled by the wing tip (ϕb) divided by the actual time spent on the downstroke (τT) or upstroke [$(1-\tau)T$], although the wing's angular velocity does not remain constant.

	Ref.	Body mass, M (kg)	Wing semi-span, b (m)	Disk loading, N_d(N m^{-2})	Stroke period, T (s)	Feathering parameter, f
			Normal hovering			
Chalcid wasp, *Encarsia formosa*	(1) (7)	$2{\cdot}5 \times 10^{-8}$	7×10^{-4}	0·16	1/370	0·025
Fruit fly, *Drosophila virilis*	(1)	2×10^{-6}	0·003	0·69	1/240	0·0137
Crane fly, *Tipula paludosa*	(1)	$2{\cdot}8 \times 10^{-5}$	0·0173	0·29	1/53	0·0036
Hover fly, *Eristalis tenax*	(1)	$1{\cdot}5 \times 10^{-4}$	0·0127	2·90	1/182	0·0056
Bumble bee, *Bombus terrestris*	(1)	$8{\cdot}8 \times 10^{-4}$	0·0173	9·18	1/156	0·0130
Moth, *Manduca sexta*	(1)	$1{\cdot}12 \times 10^{-3}$	0·050	1·40	1/29·1	0·0069
Hummingbird, *Amazilia fimbriata*	(1)	$5{\cdot}1 \times 10^{-3}$	0·059	4·57	1/35	0·0111
			Avian hovering			
Wren, *Troglodytes troglodytes*	(2)	0·01	0·085	4·32	0·084 (5)	0·175
Pied flycatcher, *Ficedula hypoleuca*	(3)	0·012	0·115	2·83	0·07	0·044
Pigeon, *Columba livia*	(4)	0·333	0·316	10·41	0·15	0·097
Mallard, *Anas platyrhynchos*	(2) (6)	1·105	0·450	17·04	0·15 (4)	0·079
Long-eared bat, *Plecotus auritus*	(1) (8)	9×10^{-3}	0·115	2·13	0·08	0·043

TABLE 1. Morphologic data for representative flying animals: (1) from Weis-Fogh (1973); (2) mass and wing data from Greenewalt (1962); (3) from Norberg (1975); (4) from Oehme & Kitzler (1975*b*); (5) author's estimate based on allometric scaling; (6) never observed to hover; (7) Reynolds number too low for vortices to persist; (8) treated aerodynamically as birds.

We may distinguish different patterns of wing motions in birds and insects which will prove important. The wake configuration is similar in the two cases, but the method of vortex-ring generation differs. The distinction is illustrated in figures 2 and 3.

A bird does little or no useful aerodynamic work during its upstroke, and the wing flexes to minimize fluid drag. All lift (and thrust in forward flight) must be generated during the downstroke. Although the downstroke only occupies a proportion τ of the stroke period T, the single ring produced must support the animal for the duration of the entire stroke, so that $T_w = T$. Typically τ is between one-third and two-thirds; Norberg (1975) observed the value $\frac{3}{7}$. This form of hovering is referred to as *avian* (figure 2*b*).

On the other hand, in *normal* hovering, typical among insects, the down- and upstrokes are symmetrical (figure 2*a*), and τ is exactly one-half. The wing tips follow figure-of-eight paths, and the wing is flipped over as it reverses direction so that the fore edge is always leading. This flip serves to 'flick off' any bound vorticity on the wing and to set up vorticity of the opposite sense, appropriate for lift generation during the following portion of the stroke. During each stroke two vortex rings are generated, so $T_w = \frac{1}{2}T$.

The distinction between the two forms of hovering arises largely as a result of the different mass scales of birds and insects. Each mode carries distinct advantages, whose effectiveness depends upon the size range (Lighthill 1977; Weis-Fogh 1977). Insects gain great advantage from their ability to store wing inertial energy elastically in the thorax, and can save a good deal of energy which would otherwise be wasted

(Weis-Fogh 1972, 1973). Despite the lack of any elastic resonance, hummingbirds also use normal hovering; for our purposes insects and hummingbirds may be grouped together.

From the definition above,

$$f = u_i^2/u_t^2 \tag{14}$$

$$= \frac{Mg}{2\rho A}\Big/\left(\frac{\pi b}{T_w}\right)^2 \tag{15}$$

$$= \frac{MgT_w^2}{2\pi^3\rho b^4} = \frac{MgT_w^2}{2\pi\rho A^2}. \tag{16}$$

For a bird $T_w = T$ and for an insect $T_w = \frac{1}{2}T$. The variation of f with disk area squared is inconvenient as it demands more accurate knowledge of the wing-span than we can usually expect. In table 1 it is likely that the high value of f for the wren is caused in part by inaccuracies in wing-span data. There is a clear tendency for f to increase with body mass, on separate scales for birds and insects because of the difference by a factor of 4 in T_w^2 between the two groups. It will be seen that there are a number of inconsistencies in the table, owing to inaccurate measurements and, in the case of the birds, lack of adequate kinematic data; the only species for which a complete reliable set is available is the pied flycatcher (Norberg 1975). There is a pressing need for a wide variety of suitable measurements of both kinematic and morphologic data.

It is important to appreciate the difference in wake generation between the birds and the insects, for although the wakes correspond, the wing motions do not; figure 3 illustrates the two cases diagramatically. Before it begins to convect downwards, the vortex sheet shed by the wings lies along the trajectory of the wings' motions. Ellington (1978) has shown that the inclination γ of each portion of the path for a hovering insect is sufficient for the induced velocity of the wake (or in our terminology the self-induced velocity of each portion of the shed vortex ring) to bring the shed vorticity to a plane. In avian hovering the starting vortex left at the beginning of the downstroke travels downwards until it combines with the stopping vortex shed by a flick of the wing at the end of the downstroke to form a plane circular ring. In both normal and avian hovering a plane circular small-cored vortex ring lying parallel to the wing disk is a good description of the final configuration of the vortex element shed by each powered stroke. Thereafter the ring travels downwards because of its own self-convection and the influence of the total velocity field of the other rings in the wake. Experiments by Magnan, Perrilliat-Botonet & Girard (1938) show vortex rings in the wake of a pigeon in slow forward flight, and photographs by Ellington (1978) show ring formation taking place for a tethered crane fly. Between them these two pieces of work provide the bulk of the experimental evidence on which this theory is based. It is hoped that similar photographs may become available for other species.

The values of f given in table 1 indicate that sample values $f = 0{\cdot}005$–$0{\cdot}015$ and $0{\cdot}05$–$0{\cdot}15$ will represent the majority of hovering animals. The most useful result that we derive is the rate of working by the animal in generating the wake, which may be compared with the simple momentum jet calculation given in §2 to estimate the tip losses associated with animal hovering.

Further details of the biological applications of the vortex-ring theory of hovering are given in Rayner (1979*b*, §2).

4. Vortex-ring theory

We use the 'classical' small-cored circular ring of Kelvin (see, for example, Lamb 1932, art. 161) to model the elements of the wake. In adopting such rings we assume, without justification, that the core radius appropriate in natural flight is sufficiently small; no more exact analytic theory is available.

A 'small-cored' vortex is defined as a vortex loop with vorticity confined to a circular core centred on the loop with cross-sectional radius small compared with the radius of curvature of the loop. The core is the region of concentrated vorticity, not the region of recirculating fluid attached 'like a bubble' to the ring. In the case of a plane circular right of radius R and cross-sectional radius $R_0 \ll R$ with circulation κ, Saffman (1970) derives the formulae

$$U_s \approx \frac{\kappa}{4\pi R}\left[\log_e\left(\frac{8R}{R_0}\right) + \bar{A} - \tfrac{1}{2}\right] \tag{17}$$

for the self-induced velocity of the ring and

$$E_s \approx \tfrac{1}{2}\rho\kappa^2 R\left[\log_e\left(\frac{8R}{R_0}\right) + \bar{A} - 2\right] \tag{18}$$

for the self-energy. An alternative derivation of these formulae is given in the appendix to II. The constant $\bar{A}$ depends upon the distribution of vorticity in the core. When the distribution is constant $\bar{A} = \frac{1}{4}$, which value we shall use; it varies otherwise between 0 and $\frac{1}{2}$. The impulse of the plane circular ring is perpendicular to the plane of the ring, and is given by

$$I = \rho\kappa\pi R^2, \tag{19}$$

independent of the core radius. Detailed mathematical studies (Fraenkel 1970; Norbury 1973) have verified that (17) and (18) are valid asymptotically as $R_0/R \to 0$; in addition Norbury has shown that the asymptotic approximations remain accurate for R_0/R less than about $\frac{1}{4}$. All of these theories assume that the ring conserves its circulation and does not deform; Maxworthy (1972, 1977) has shown that an isolated ring expands as it travels, and leaves some of its vorticity in a narrow wake. However, for our purposes the approximations (17) and (18) will be sufficient. We also neglect any effects of viscous dissipation of vorticity from the ring cores.

Away from the core of a ring we calculate the induced velocity field from the Biot–Savart law (20), since the vortex core can be approximated to a line vortex:

$$\mathbf{u}(\mathbf{x}) = -\frac{\kappa}{4\pi}\oint \frac{(\mathbf{x}-\mathbf{X}(s)) \wedge \mathbf{t}(s)}{|\mathbf{x}-\mathbf{X}(s)|^3}\, ds, \tag{20}$$

where $\mathbf{u}(\mathbf{x})$ is the velocity induced at $\mathbf{x}$ by a vortex ring of strength κ, with circumference parameterized by s. Consider the velocity $\mathbf{u}(\mathbf{x})$ at $\mathbf{x} = (r, 0, h)$ due to a ring of radius R centred at the origin (figure 4); $\mathbf{u}$ is relative to still fluid, independent of the motion of the ring itself. Then

$$\mathbf{u}(\mathbf{x}) = \frac{\kappa R}{4\pi}\int_0^{2\pi} \frac{(h\cos\theta, h\sin\theta, R - r\cos\theta)}{[r^2 - 2rR\cos\theta + R^2 + h^2]^{\frac{3}{2}}}\, d\theta; \tag{21}$$

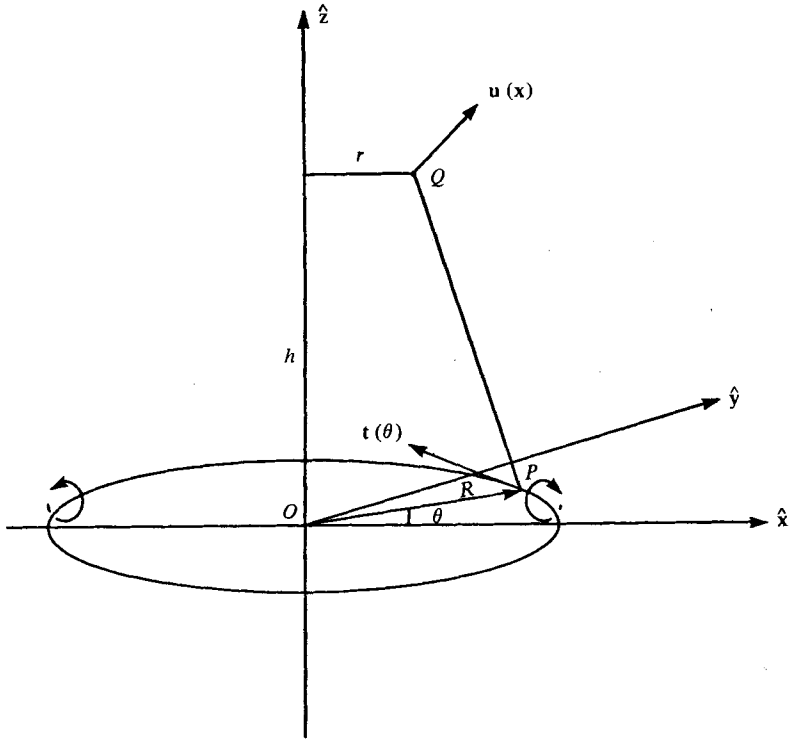

FIGURE 4. Notation for calculation of the velocity field induced by a circular vortex ring with centre O, radius R and an infinitesimal core, in Cartesian co-ordinates. Point on ring P, $\mathbf{X} = R(\cos\theta, \sin\theta, 0)$. Field point Q, $\mathbf{x} = (r, 0, h)$; $s = R\theta$; $\mathbf{t} = d\mathbf{X}/ds = (-\sin\theta, \cos\theta, 0)$.

$\mathbf{u}(\mathbf{x}).\hat{\mathbf{y}} = 0$ because of symmetry about the $\hat{\mathbf{z}}$ axis. We define functions I_1 and I_2 such that

$$\left.\begin{aligned} \mathbf{u}.\hat{\mathbf{x}} &= (\kappa Rh/4\pi)\, I_2(r, R, h) \\ \text{and} \qquad \mathbf{u}.\hat{\mathbf{z}} &= (\kappa R/4\pi)\,(RI_1(r, R, h) - rI_2(r, R, h)). \end{aligned}\right\} \tag{22}$$

I_1 and I_2 can be evaluated in terms of the complete elliptic integrals K and E, defined as

$$K(e) = \int_0^{\frac{1}{2}\pi} (1 - e^2\cos^2\bar{\theta})^{-\frac{1}{2}}\, d\bar{\theta}, \quad E(e) = \int_0^{\frac{1}{2}\pi} (1 - e^2\cos^2\bar{\theta})^{\frac{1}{2}}\, d\bar{\theta}. \tag{23}$$

With the eccentricity e given by

$$e^2 = 4rR[(r+R)^2 + h^2]^{-1}, \tag{24}$$

we derive

$$I_1(r, R, h) = \int_0^{2\pi} [r^2 + R^2 + h^2 - 2rR\cos\theta]^{-\frac{3}{2}}\, d\theta \tag{25}$$

$$= 4[(r+R)^2 + h^2]^{-\frac{3}{2}} \int_0^{\frac{1}{2}\pi} (1 - e^2\cos^2\bar{\theta})^{-\frac{3}{2}}\, d\bar{\theta}. \tag{26}$$

From tables of integrals (Gradshteyn & Rhyzhik 1965, §3.84), we define $G(e)$ such that

$$I_1(r, R, h) = 4G(e)\,[(r+R)^2 + h^2]^{-\frac{3}{2}}, \tag{27}$$

where

$$G(e) = E(e)\,(1-e^2)^{-1}. \tag{28}$$

Similarly,

$$I_2(r,R,h) = 4[(r+R)^2+h^2]^{-\frac{3}{2}} \int_0^{\frac{1}{2}\pi} \cos 2\bar{\theta}(1-e^2\cos^2\bar{\theta})^{-\frac{3}{2}}\,d\bar{\theta} \tag{29}$$

$$= 4H(e)\,[(r+R)^2+h^2]^{-\frac{3}{2}}, \tag{30}$$

where

$$H(e) = \frac{1}{e^2}\left(\frac{2-e^2}{1-e^2}\,E(e) - 2K(e)\right). \tag{31}$$

G and H are evaluated numerically using standard routines to calculate E and K. If $e \to 1$, $E(e) \to 1$ and $K(e) \sim \log_e(4(1-e^2)^{-\frac{1}{2}}) + O((1-e^2)^{\frac{1}{2}})$; the logarithmic singularity corresponds to the close approach of $\mathbf{x}$ to the vortex core. If $e \to 0$, corresponding to points near the z axis or to points in the far field, the following expressions are used for G and H:

$$\left.\begin{aligned} G(e) &= \tfrac{1}{2}\pi(1+\tfrac{3}{4}e^2+\tfrac{45}{64}e^4) \quad \text{for} \quad e^2 < 0{\cdot}05, \\ H(e) &= \tfrac{3}{16}\pi e^2(1+\tfrac{5}{4}e^2) \quad \text{for} \quad e^2 < 0{\cdot}01. \end{aligned}\right\} \tag{32}$$

With the aid of (28) and (31) we can express the velocity field in cylindrical polar co-ordinates:

$$\left.\begin{aligned} \mathbf{u} &= u_r\hat{\mathbf{x}} + u_z\hat{\mathbf{z}}, \\ u_r &= \frac{\kappa Rh}{4\pi}\,\frac{4}{[(r+R)^2+h^2]^{\frac{3}{2}}}\,H(e), \\ u_z &= \frac{\kappa R}{4\pi}\,\frac{4}{[(r+R)^2+h^2]^{\frac{3}{2}}}\,(RG(e)-rH(e)), \end{aligned}\right\} \tag{33}$$

with e given by (24). It will prove convenient to non-dimensionalize lengths with respect to the initial ring radius $R'b$; lengths on this scale will be denoted by an over bar. The wing-disk radius b will not necessarily be the same as the initial radius $R'b$ of a vortex ring. Values of R' are calculated in § 5. We also introduce a two-component vector $\bar{\mathbf{p}} = (\bar{R}, \bar{Z})$, where $\bar{R}R'b$ is the radius of a ring and $\bar{Z}R'b$ the ordinate on the z axis. We can thus express the velocity field induced at the point $\bar{\mathbf{x}} = (\bar{r}, 0, \bar{z})$ by a ring $\bar{\mathbf{p}}$ as

$$\mathbf{u}(\bar{\mathbf{x}};\mathbf{p}) = \frac{\kappa}{4\pi R'b}\,\overline{\mathbf{U}}(\bar{\mathbf{x}};\bar{\mathbf{p}}),$$

where

$$\left.\begin{aligned} \overline{\mathbf{U}}\,.\,\hat{\mathbf{x}} &= \frac{4\bar{R}(\bar{z}-\bar{Z})\,H(e)}{[(\bar{r}+\bar{R})^2+(\bar{z}-\bar{Z})^2]^{\frac{3}{2}}}, \\ \overline{\mathbf{U}}\,.\,\hat{\mathbf{z}} &= \frac{4\bar{R}(\bar{R}G(e)-\bar{r}H(e))}{[(\bar{r}+\bar{R})^2+(\bar{z}-\bar{Z})^2]^{\frac{3}{2}}} \end{aligned}\right\} \tag{34}$$

and

$$e^2 = 4\bar{r}\bar{R}[(\bar{r}+\bar{R})^2+(\bar{z}-\bar{Z})^2]^{-1}.$$

We assume that the rings forming the wake have small, but finite, core radius; we must allow the core radius to vary as the ring size varies to keep the volume of the core constant. Initially the ring has radius $R'b$ and core radius $\bar{R}_0'R'b$, where $\bar{R}_0' \lesssim \frac{1}{4}$. At all other times the core radius $\bar{R}_0R'b$ and ring radius $\bar{R}R'b$ must satisfy the continuity equation

$$2\pi\bar{R} \times \pi\bar{R}_0^2 = 2\pi \times \pi\bar{R}_0'^2; \tag{35}$$

$\bar{R} = 1$ initially for each ring.

Suppose now that there are n vortex rings present, denoted by $\bar{\mathbf{p}}_i (1 \leqslant i \leqslant n)$, each with circulation κ. The induced velocity at $\bar{\mathbf{x}}$ due to this family is given by

$$\mathbf{u}(\bar{\mathbf{x}}) = \frac{\kappa}{4\pi b \bar{R}'} \sum_{i=1}^{n} \overline{\mathbf{U}}(\bar{\mathbf{x}}; \bar{\mathbf{p}}_i) \tag{36}$$

provided that $\bar{\mathbf{x}}$ is not within a vortex core. The velocity induced on a member $\bar{\mathbf{p}}_j$ of the family is given by

$$\mathbf{u}(\bar{\mathbf{p}}_j) = \frac{\kappa}{4\pi b \bar{R}'} \left\{ \overline{U}_s(\bar{\mathbf{p}}_j)\, \mathbf{z} + \sum_{i=1,\, i \neq j}^{n} \overline{\mathbf{U}}(\bar{\mathbf{x}}; \bar{\mathbf{p}}_i) \right\}, \tag{37}$$

where $\overline{U}_s(\bar{\mathbf{p}}_j)$ is the self-induced velocity of ring $\bar{\mathbf{p}}_j$, given by, from (17),

$$\overline{U}_s(\bar{\mathbf{p}}_j) = \bar{R}_j^{-1} \left\{ \log_e \left(\frac{8\bar{R}_j}{\bar{R}_{0j}} \right) - \tfrac{1}{4} \right\}; \tag{38}$$

$\bar{R}_{0j}$ and $\bar{R}_j$ are related by

$$\bar{R}_j \bar{R}_{0j}^2 = \bar{R}_0'^2 \tag{39}$$

[from (35)], since R' and $\bar{R}_0'$ are the same for all rings.

The theory outlined above is essentially that of Kelvin. If only two rings are present it predicts that they pass through each other alternately until the effects of viscosity have diffused the vorticity away (Batchelor 1967, p. 523). Maxworthy (1972) suggests on the basis of experimental results that the rearward ring is drawn through the centre of the foremost ring and becomes 'wrapped' around it to produce one stronger ring. The model displays both patterns, depending on the size and strength of the rings. Attempts have been made in the model to allow adjacent rings to amalgamate should they become sufficiently close, but not enough is known about the behaviour to develop a reliable algorithm; the results without any form of amalgamation are easier to interpret, but require a greater length of computing time.

The question of stability, either of a single ring or of the whole system, is important when we calculate the energy involved. Widnall & Sullivan (1973) and Widnall & Tsai (1977) have shown that a wave-like instability develops around the circumference of a single ring. A chain of equally spaced similar coaxial rings has been investigated by Levy & Forsdyke (1927), and was found to be unstable to perturbations parallel to the axis; we find some instability of this kind, but the chain of rings does not disintegrate as their calculations suggest it should. We neglect the possibility of the breakup of a single ring through radial perturbations, with the justification that this will occur only when the ring is sufficiently far along the wake to have little effect on other rings near the wing disk or the contraction neck. By the same argument the energy of the system cannot be significantly affected by any breakup or instability far from the wing disk.

One of the most useful indications of an animal's flight performance is the power consumption, for this is directly dependent upon the fuel reserves and the chemical efficiency of the muscles. A significant portion of the hovering energy cost is involved in generating fluid momentum to support the animal's weight, and is termed the induced power. We estimate this from the family of vortex rings by calculating the energy increment in the wake when a single ring is added to the chain at the wing disk.

With vorticity $\boldsymbol{\omega}(\mathbf{x})$ distributed over a volume V, the total kinetic energy of the fluid flow induced is given by

$$E = \frac{1}{8\pi} \rho \iiint_V \iiint_V \frac{\boldsymbol{\omega}(\mathbf{x}) \cdot \boldsymbol{\omega}(\mathbf{x}')}{|\mathbf{x} - \mathbf{x}'|}\, d^3x\, d^3x' \tag{40}$$

(Lamb 1932, art. 153). When the volume V consists of n separate closed vortex loops of circulation κ we can rewrite (40) as

$$E = \frac{1}{8\pi}\rho\kappa^2 \sum_{i=1}^{n} \left\{ E_{s,i} + \sum_{\substack{j=1 \\ j\neq i}}^{n} \oint_i \oint_j \frac{\mathbf{t}_i(\mathbf{x}) \cdot \mathbf{t}_j(\mathbf{x}')}{|\mathbf{x}-\mathbf{x}'|}\, ds\, ds' \right\}, \tag{41}$$

where the first term within the curly brackets accounts for the self-energy of the loops. It is not helpful to discuss the total energy of the wake when many rings are present since this will increase indefinitely. The increment in energy between the generation of successive rings tends to a finite value, and is readily calculated. Suppose that there are n rings present in the wake, $\{\bar{\mathbf{p}}_i; 1 \leqslant i \leqslant n\}$, and that a further ring $\bar{\mathbf{p}}_{n+1} = (1, 0)$ is added on the wing disk. Then the energy increment ΔE for time T_w is given by

$$\Delta E = \tfrac{1}{2}\rho\kappa^2 b R' \left\{ \bar{E}_s + \sum_{i=1}^{n} \bar{E}_m(\bar{\mathbf{p}}_{n+1}; \bar{\mathbf{p}}_i) \right\}, \tag{42}$$

where the self-energy of the new ring is

$$\bar{E}_s = \log_e(8/\bar{R}_0') - \tfrac{7}{4} \tag{43}$$

from (18), and the mutual energy $\bar{E}_m$ between ring i and the new ring $n+1$ is

$$\bar{E}_m(\bar{\mathbf{p}}_{n+1}; \bar{\mathbf{p}}_i) = \frac{1}{2\pi b R'} \oint_i \oint_{n+1} \frac{\mathbf{t}_i \cdot \mathbf{t}_{n+1}}{|\mathbf{x}_i - \mathbf{x}_{n+1}|}\, ds_i\, ds_{n+1}, \tag{44}$$

with notation as in figure 5. From (44)

$$\bar{E}_m(\bar{\mathbf{p}}_{n+1}; \bar{\mathbf{p}}_i) = \frac{1}{2\pi} \bar{R}_i \iint_0^{2\pi} \cos(\phi - \phi') [1 + \bar{Z}_i^2 + \bar{R}_i^2 - 2\bar{R}_i \cos(\phi - \phi')]^{-\frac{1}{2}}\, d\phi\, d\phi' \tag{45}$$

$$= \frac{2\bar{R}_i}{[\bar{Z}_i^2 + (\bar{R}_i + 1)^2]^{\frac{1}{2}}} \int_0^{\pi} \cos 2\psi (1 - e^2 \cos^2\psi)^{-\frac{1}{2}}\, d\psi, \tag{46}$$

where

$$e^2 = 4\bar{R}_i (\bar{Z}_i^2 + (\bar{R}_i + 1)^2)^{-1}. \tag{47}$$

In terms of complete elliptic integrals

$$\bar{E}_m(\bar{\mathbf{p}}_{n+1}; \bar{\mathbf{p}}_i) = \frac{4\bar{R}_i J(e)}{[\bar{Z}_i^2 + (\bar{R}_i + 1)^2]^{\frac{1}{2}}}, \tag{48}$$

where

$$J(e) = e^{-2}\{(2 - e^2) K(e) - 2E(e)\}.$$

For $e^2 < 0{\cdot}05$ we use the expression

$$J(e) = \tfrac{1}{16}\pi e^2 (1 + \tfrac{3}{4} e^2 + \tfrac{75}{128} e^4). \tag{49}$$

By substitution in (42) we can readily calculate the rate of energy increment $\Delta E/T_w$ for this wake structure, which we express non-dimensionally as σ by dividing by the energy rate $P_{i,M}$ for the momentum jet (12).

By this definition, the energy rate σ when n rings are present is

$$\sigma = \frac{\Delta E}{T_w} \Big/ P_{i,M}, \tag{50}$$

or by substitution from (42),

$$\sigma = \tfrac{1}{2}\rho\kappa^2 b R' \left(\bar{E}_s + \sum_{i=1}^{n} \bar{E}_m \right) \Big/ T_w M g \left(\frac{Mg}{2\rho A} \right)^{\frac{1}{2}}. \tag{51}$$

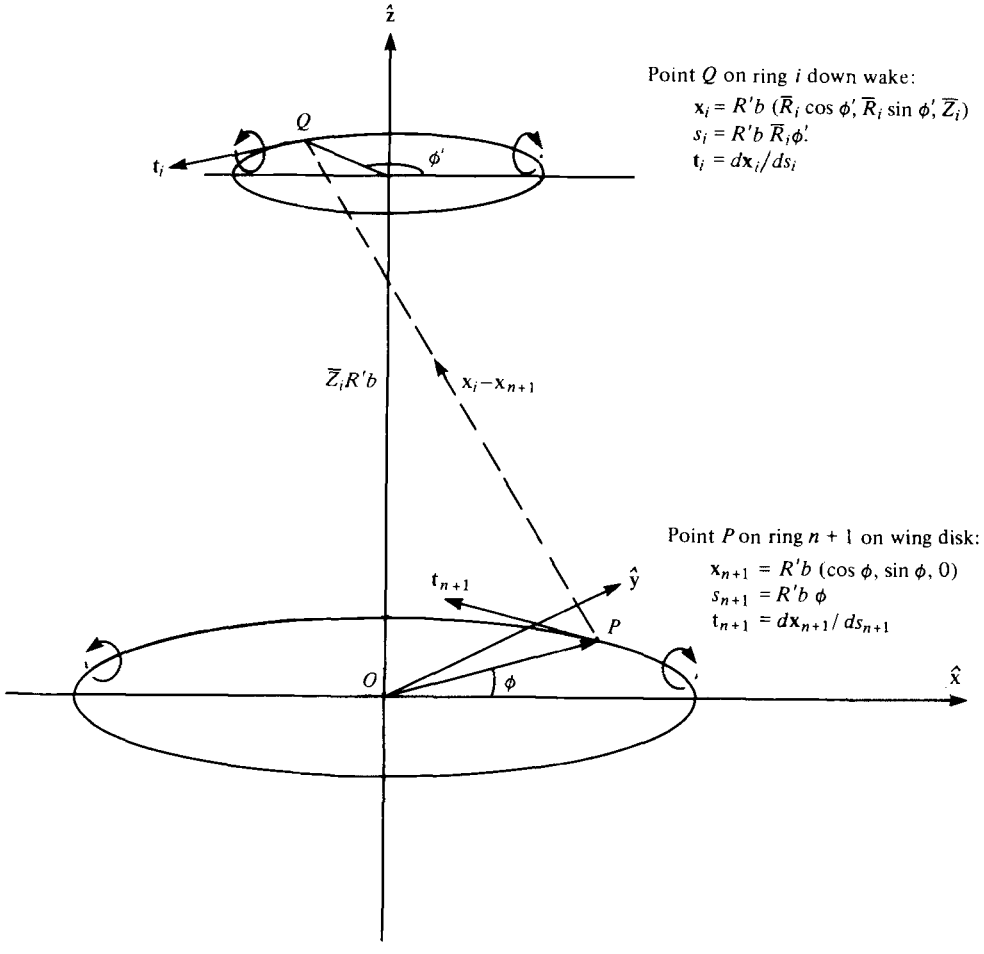

FIGURE 5. Notation for calculation of interactive (mutual) kinetic energy between a vortex ring $n+1$ on the wing disk and a ring i far down the wake.

In the application to animal hovering we determine κ from the momentum of a single initial vortex ring, which must support the animal for time T_w. This momentum is given by circulation times ring area times fluid density; it is vertical because the ring is planar and horizontal. The impulse required to generate this ring in the presence of vorticity elsewhere in the field is the same as the impulse required to generate the ring in isolation. The rate of increase of wake momentum, i.e. the impulse of a single ring divided by T_w, must balance the force which the wake must provide, i.e. the animal's weight. Therefore

$$\kappa\rho A R'^2/T_w = Mg; \tag{52}$$

by substituting for κ from (52) into (51), we find that

$$\sigma = f^{\frac{1}{2}} R'^{-3} \left(\bar{E}_s + \sum_{i=1}^{n} \bar{E}_m\right). \tag{53}$$

It will prove useful to rescale f as

$$f' = fR'^{-4}, \tag{54}$$

which is equivalent to redefining f in (16), with A replaced by R'^2A; then

$$\sigma = f'^{\frac{1}{2}}R'^{-1}\left(\bar{E}_s + \sum_{i=1}^{n} \bar{E}_m\right) \tag{55}$$

is the non-dimensional energy rate for the vortex wake of a hovering animal. The induced power is given by $P_i = \sigma P_{i,M}$. Strictly, σ as defined in (55) should be the limit as n becomes large. In practice σ converges rapidly to a definite limit, and does not change as further rings are released.

5. The wake model

We have seen how the wake of an animal in hovering flight may be modelled by a chain of stacked coaxial circular vortex rings. A first approximation to the configuration is the momentum jet generated by an ideal actuator disk. The object of the calculations described in this section is the construction of a numerical model of the wake, which will predict the development of its shape with time. If we know the array of ring positions $\{\bar{\mathbf{p}}_i, 1 \leqslant i \leqslant n\}$ when n rings are present we can calculate the induced power required to generate the wake by the method outlined at the end of §4.

If we assume that an ideal equilibrium configuration of the wake exists, we can reasonably visualize it by breaking up the boundary of a momentum jet into discrete vortex rings. The wake is then a semi-infinite chain of rings, of equal radius (and equally spaced) in the far field, and with a contraction region just below the wing disk. This configuration would have to be *self-consistent* in the sense that it deforms 'into itself' over a single wing cycle; any member of the family of rings travels and deforms to become the next in the chain, and a further ring is added on the wing disk.

The problem can be conceived as that of finding the array $\{\bar{\mathbf{p}}_i(t), 1 \leqslant i \leqslant n\}$ such that $\bar{\mathbf{p}}_i(t+T_w) = \bar{\mathbf{p}}_{i+1}(t)$ for all t an integer multiple of T_w. Levy & Forsdyke (1927) have demonstrated that the semi-infinite chain of vortex rings which should constitute at least the far-field wake is unstable. Therefore any attempts to relax onto the solution from a nearby estimate are unlikely to be successful.

An alternative approach is to start generating equal rings at equal time intervals, with initially all fluid at rest. This situation is possibly more realistic; it enables us to trace the evolution of the wake with time, and to demonstrate that the ideal semi-infinite chain conjectured above is not usually observed. We follow this procedure.

We shall observe that the far-field wake generally breaks up, unless f' is very large. The near field, which has a dominant influence on the energy, converges to a constant contraction and steady ring spacing; in this region the solution *is* self-consistent. We also find that a large vortex ring is formed at the lower open end of the tube; this is the agglomeration of several rings, and encourages fluid recirculation outside the boundary of the wake. Note that the term boundary now refers to the trajectory of the vortex ring centres, and that only in the case of small f' is the boundary similar to a vortex sheet within which all flow is confined. The bound ring is similar to the ring found at the top of a rising plume of lighter fluid; its presence is suggested by photographs of the crane fly by Ellington (1978). It becomes less pronounced as f' increases. To clarify these points, a diagram of a typical wake configuration is given in figure 7 (*a*).

We trace the growth of the wake as follows: suppose that the wake has been growing

for time t $[(n-1)\,T_w \leqslant t < nT_w]$; there are n rings present, each specified (as in §4) by $R'b\bar{\mathbf{p}}_j(t)$ $(1 \leqslant j \leqslant n)$. Then the configuration at time $t+\delta t$ is given approximately by

$$R'b\bar{\mathbf{p}}_j(t+\delta t) = R'b\bar{\mathbf{p}}_j(t) + \delta t \frac{\kappa}{4\pi R'b} \{\overline{\mathbf{U}}_s(\bar{\mathbf{p}}_j(t))\,\hat{\mathbf{z}} + \sum_{i \neq j} \overline{\mathbf{U}}\,(\bar{\mathbf{p}}_j(t); \bar{\mathbf{p}}_i(t))\}, \tag{56}$$

where the velocity terms on the right-hand side are defined in (37). We may add to them a further term,

$$\overline{\mathbf{U}}_0(\bar{\mathbf{p}}_j(t)) = \frac{\kappa}{4\pi R'b} f_v(t-(n-1)\,T_w)\,\overline{\mathbf{U}}(\bar{\mathbf{p}}_j(t); \bar{\mathbf{p}}_{n+1}), \tag{57}$$

synthesizing the effect of the bound vorticity on the wing disk during the growth of ring $n+1$; $\kappa f_v(t)$ is the supposed dependence of the bound vortex strength on time; by setting $\bar{\mathbf{p}}_{n+1} = (1, 0)$ we indicate that we assume that this bound wing vorticity has circular symmetry. The assumption is necessary as azimuthal symmetry of the wake is vital to this argument.

We allow L time steps in the interval T_w between the generation of successive rings, and indicate the step reached during a single cycle by a superscript $l (0 < l < L)$; then $\delta t = T_w/L$. We non-dimensionalize (56) by dividing by $R'b$, to define the iterative procedure

$$\bar{\mathbf{p}}_j^l = \bar{\mathbf{p}}_j^{l-1} + \frac{\pi f'}{2L} \left\{\overline{\mathbf{U}}_s(\bar{\mathbf{p}}_j^{l-1})\,\mathbf{z} + \sum_{\substack{i=1 \\ i \neq j}}^{n} \overline{\mathbf{U}}\,(\bar{\mathbf{p}}_j^{l-1}; \bar{\mathbf{p}}_j^{l-1}) + f_v\left(\frac{(l-1)\,T_w}{L}\right) \overline{\mathbf{U}}\,(\bar{\mathbf{p}}_j^{l-1}; \bar{\mathbf{p}}_{n+1})\right\}, \tag{58}$$

which traces the evolution of $\mathbf{p}_j$. At the end of each stroke, when $l = L$, n is incremented, a further ring is added $(\mathbf{p}_{n+1}^0 = (1, 0))$, and l is reset to zero. The system depends solely on the parameters f' and $\bar{R}_0$, and upon the choice of f_v and L. Greater accuracy can be achieved by increasing L, but at the cost of greater computation time; a value $L = 8$ proved suitable. At the completion of a cycle, (55) can be used to calculate the rate of working averaged over that cycle.

We must now consider the appropriate values of R', which depend, as we have mentioned in §1, on the distribution of wing circulation. The feathering parameter f is determined for the animal concerned; f is related to the modified feathering parameter f' by (54), and it is upon f' that the wake depends. The variation of f' with R'^{-4} allows R' to influence the resulting configuration significantly, so that an accurate value is important. R' is the scale for all wake dimensions, so that it will also affect the size of the resulting wake pattern. However, exact derivation of R' would be complicated, and represents an important calculation in its own right; we do no more here than suggest a simple algorithm for its estimation. The initial core radius $\bar{R}_0'$ is harder to derive, but has a less important effect on the shape of the wake, and sample values will suffice.

As each wing moves through the air it leaves a trailing vortex sheet; the extremities of the sheet are closed by the starting and stopping vortices. Initially an element of the sheet lies on the trace of the wing, but it will move immediately under the influence of the remainder of the sheet and of the bound vorticity on the wing. We assume that the final configuration of the vorticity forming the sheet is a circular vortex ring. The size of this ring is determined by assuming that it has the same impulse as the vortex sheet; the circulation is the same as the total circulation κ in the sheet. If the wing circulation varies during the stroke we are not able to determine the strength of the

vortex ring by a straightforward calculation, so we assume that the circulation varies only with wing-span. We assume also that the vortex sheet initially forms a plane 'butterfly'-shaped sector of the wing disk matching the area mapped out by the wings.

Let the wing circulation be given by $\Gamma(\zeta)$, with $\Gamma(1) = 0$, where ζ $(0 \leqslant \zeta \leqslant 1)$ is a measure of radius on the wing. The wings beat from $-\frac{1}{2}\phi$ to $\frac{1}{2}\phi$. An annular sector of the vortex sheet with radius between $b\zeta$ and $b(\zeta+\delta\zeta)$ has strength $-\Gamma'(\zeta)\,\delta\zeta$. The contribution δI to the total impulse of the sheet from this annulus is

$$\delta I(\zeta) = -\rho\Gamma'(\zeta)\,\delta\zeta\,\pi b^2\zeta^2\phi/\pi \tag{59}$$

$$= -\rho b^2\phi\zeta^2\Gamma'(\zeta)\,\delta\zeta. \tag{60}$$

Only the portion of the sheet for which $\Gamma'(\zeta) < 0$, say $\zeta_0 < \zeta \leqslant 1$, where $0 \leqslant \zeta_0$, can roll up into a vortex ring producing useful mass support. The remainder of the sheet rolls up into a smaller ring of the opposite circulation which will interact with the animal's body and will presumably be annihilated. This opposing ring has small radius, therefore its energy and impulse are small; to simplify the calculation they will be ignored. The total useful impulse is then

$$I = -\rho b^2\phi \int_{\zeta_0}^{1} \zeta^2\Gamma'(\zeta)\,d\zeta \tag{61}$$

$$= \rho b^2\phi \left[2\int_{\zeta_0}^{1} \zeta\Gamma(\zeta)\,d\zeta + \zeta_0^2\,\Gamma(\zeta_0)\right]. \tag{62}$$

The total circulation in this part of the sheet,

$$\kappa = -\int_{\zeta_0}^{1} \Gamma'(\zeta)\,d\zeta \tag{63}$$

$$= \Gamma(\zeta_0) > 0, \tag{64}$$

will be the circulation of the vortex ring. We determine the initial ring radius $R'b$ by balancing impulses between the ring and the sheet; therefore

$$\pi R'^2 b^2\rho\Gamma(\zeta_0) = \rho b^2\phi \left[2\int_{\zeta_0}^{1} \zeta\Gamma(\zeta)\,d\zeta + \zeta_0^2\,\Gamma(\zeta_0)\right], \tag{65}$$

from which we can write

$$R'^2 = \lambda_0 \left[\frac{2}{\Gamma(\zeta_0)}\int_{\zeta_0}^{1} \zeta\Gamma(\zeta)\,d\zeta + \zeta_0^2\right], \tag{66}$$

where $\lambda_0 = \phi/\pi$.

Sample values of R'^2 for some likely circulation distributions are given in table 2. For a semi-elliptic wing a reasonable estimate of R' (allowing for $\lambda_0 < 1$) would be 0·7 or 0·8. Sample values of $\bar{R}_0' = 0{\cdot}1$, 0·171 and 0·225 span the likely range of values of the core radius, and we do not attempt to find a more accurate value.

In the interval between successive strokes of the wings it is necessary to synthesize the effect of the bound vorticity on the wings, which will in time become part of the next vortex ring to be shed. This is the reason for the function $f_v(t)$ in (58); in the form in which it appears, it is assumed that the bound vorticity has circular symmetry. We must have $f_v = 0$ when $t = 0$; f_v takes its maximum value of 1 when $t = T_w$, and

$\Gamma(\zeta)/\Gamma_0$	$\zeta_0\ [\Gamma'(\zeta_0) = 0]$	R'^2/λ_0
1	0	≈ 1
$(1-\zeta^2)^{\frac{1}{2}}$	0	$\frac{2}{3}$
$\zeta(1-\zeta^2)^{\frac{1}{2}}$	$\sqrt{\frac{1}{3}}$	0·923
$\zeta^2(1-\zeta^2)^{\frac{1}{2}}$	$\sqrt{\frac{1}{2}}$	0·967
$1-\zeta$	0	$\frac{1}{3}$
$\zeta(1-\zeta)$	$\frac{1}{2}$	0·708
$1-\zeta^2$	0	$\frac{1}{2}$
$\zeta(1-\zeta^2)$	$\sqrt{\frac{1}{2}}$	0·759
* $\begin{cases} 1 & \text{for } \zeta < \frac{1}{2} \\ 4\zeta(1-\zeta) & \text{for } \zeta > \frac{1}{2} \end{cases}$	0	0·708
$\begin{cases} \zeta & \text{for } \zeta < \frac{1}{2} \\ 4\zeta^2(1-\zeta) & \text{for } \zeta > \frac{1}{2} \end{cases}$	$\frac{2}{3}$	0·808

TABLE 2. Sample values of R'^2/λ_0 for typical circulation distributions $\Gamma(\zeta)/\Gamma_0$. The distribution marked * corresponds to the form of a bird's wing chord given by Oehme & Kitzler (1975*a*); that beneath it is proportional to wing-span times chord; in hovering this is proportional to local wing velocity times chord, and on a simple theory would be a good estimate of the circulation distribution. λ_0 is a measure of the stroke amplitude ($\lambda_0 = (\phi/\pi)^{\frac{1}{2}}$); for most species λ_0^2 will lie between 0·67 and 1 (Weis-Fogh 1973).

grows steadily in between. One extreme form for f_v, which has little physical significance, is linear growth

$$f_{v,1}(t) = t/T_w, \tag{67}$$

while the other is a sudden step-like growth

$$f_{v,2}(t) = \begin{cases} 0 & \text{for } t < T_w - \epsilon, \quad (68a) \\ 1 & \text{for } T_w - \epsilon < t < T_w, \quad (68b) \end{cases}$$

where $\epsilon < T_w/L$. A more realistic form, with some physical significance as it is allied to observed wing velocities, is the semi-sine-squared form

$$f_{v,3}(t) = \begin{cases} 0 & \text{for } t < \frac{1}{2}T_w, \quad (69a) \\ \sin^2 \pi(t/T_w - \frac{1}{2}) & \text{for } \frac{1}{2}T_w < t < T_w. \quad (69b) \end{cases}$$

The effects of each of these three possibilities are considered. The shape of the wake when f' is large depends significantly on f_v, suggesting that we need to know more about conditions on the wing disk, but the energy rate is only very weakly dependent on f_v. When f' is small f_v has very little influence on the wake configuration.

The model described above has been applied for a range of values of f' between 0·001 and 1, so that all realistic combinations of f and R' are covered, and with sufficient combinations of the other parameters ($\bar{R}'_0$, L and f_v) to ensure that all possibilities have been covered. The combination with $\bar{R}'_0 = 0{\cdot}171$, $L = 8$ and $f_v = f_{v,3}$ is regarded as the average or most representative. The results are described in the following sections. Each calculation required about 40–50 iterations (wing-strokes) for convergence to be established; large values of f' required fewer steps, while the smallest f' required many more. In general σ converges faster than the wake geometry, since most geometrical instabilities occur in the far field. For $f' = 0{\cdot}01$, σ converges after about 30 iterations, while for $f' = 0{\cdot}5$, $\bar{E}_s$ is large compared with the mutual energy with rings away from the contraction region and only 3 or 4 strokes are needed for convergence of σ.

For small f' the wake is close to the momentum jet generated by an actuator disk of area $A' = \pi R'^2 b^2$. Note that this area A' is different from the area A used in §2, and with which $P_{i,M}$ was defined. The induced power for this jet is $P'_{i,M} = P_{i,M}/R'$. The limit of the wake at large times as f' tends to zero should be identically this momentum jet. However, since for very small f' the wake grows too slowly, it has not been possible to do more numerically than to indicate the general truth of this supposition. For moderately small f' ($\approx 0{\cdot}005$) the vortex wake is similar to the momentum jet (figure 7*a*) in the contraction region, and moreover σ is close to $1/R'$, so that $P'_{i,M}$ is then a good estimate of the induced power.

Calculations were performed on the IBM-370 at Cambridge, with graphical output of the wake configuration from which the ring spacing and far-field radius were measured. Each calculation took between 60 and 120 s of computing time, so that the number of applications was forced to be limited. A selection of the calculations was allowed to proceed until about 125 rings were present (about 20 min) with no sign of change in the convergence of the wake or in the value of σ, and with no large-scale instability becoming evident.

The information that we record is the energy rate (non-dimensional induced power) σ, the areal contraction ratio λ, and the spacing δ between successive rings just below the contraction neck; λ is the ratio of the cross-sectional area of the wake (at either the narrowest point, or when it has settled to a steady value) to the initial ring area $\pi R'^2 b^2$.

We can relate λ to a theoretical estimate $\bar{d}$ of $\bar{\delta}$ by calculating the spacing of an infinite chain of equally spaced identical rings of radius $\bar{R}R'b = \lambda^{\frac{1}{2}}R'b$ and the same circulation κ [as in (52)] as each ring in the vortex wake. Locally the vortex wake where we record $\bar{\delta}$ is similar to a chain of identical rings. Since the velocity field falls off rapidly the estimate $\bar{d}$ for an infinite chain should be close to the measured value $\bar{\delta}$. The calculation gives a valuable check that the wake model converges to a realistic solution.

A ring in the centre of this infinite chain will appear to be sandwiched between two identical but opposing semi-infinite chains. Let the separation between any two adjacent rings be $\bar{d}R'b$; in time T_w a ring travels this distance under the combined effects of mutual and self-induced velocities. Relative to fluid at rest at infinity each wake element will appear to travel along the wake with velocity $\bar{d}R'b/T_w$. By using (37) with $\bar{\mathbf{p}}_j = (\bar{R}, j\bar{d})$, and noting that the two opposing semi-infinite chains induce only a velocity component parallel to the chain, the ring velocity must satisfy

$$\frac{\kappa}{4\pi bR'}\left\{\bar{U}_s(\bar{\mathbf{p}}_0) + 2\sum_{j=1}^{\infty}\bar{\mathbf{U}}(\bar{\mathbf{p}}_0;\bar{\mathbf{p}}_j).\hat{\mathbf{z}}\right\} = \frac{\bar{d}R'b}{T_w}. \tag{70}$$

From (38) and (39),

$$\bar{U}_s(\bar{\mathbf{p}}_0) = \bar{R}^{-1}\left(\log_e\frac{8\bar{R}^{\frac{3}{2}}}{\bar{R}'_0} - \tfrac{1}{4}\right). \tag{71}$$

The mutual velocity component

$$\bar{U}_m = 2\sum_{j=1}^{\infty}\bar{\mathbf{U}}(\bar{\mathbf{p}}_0;\bar{\mathbf{p}}_j).\hat{\mathbf{z}} \tag{72}$$

may be written after (34) as

$$\bar{U}_m = 8\bar{R}^2\sum_{j=1}^{\infty}(G(e)-H(e))(4\bar{R}^2+j^2\bar{d}^2)^{-\frac{3}{2}}, \tag{73}$$

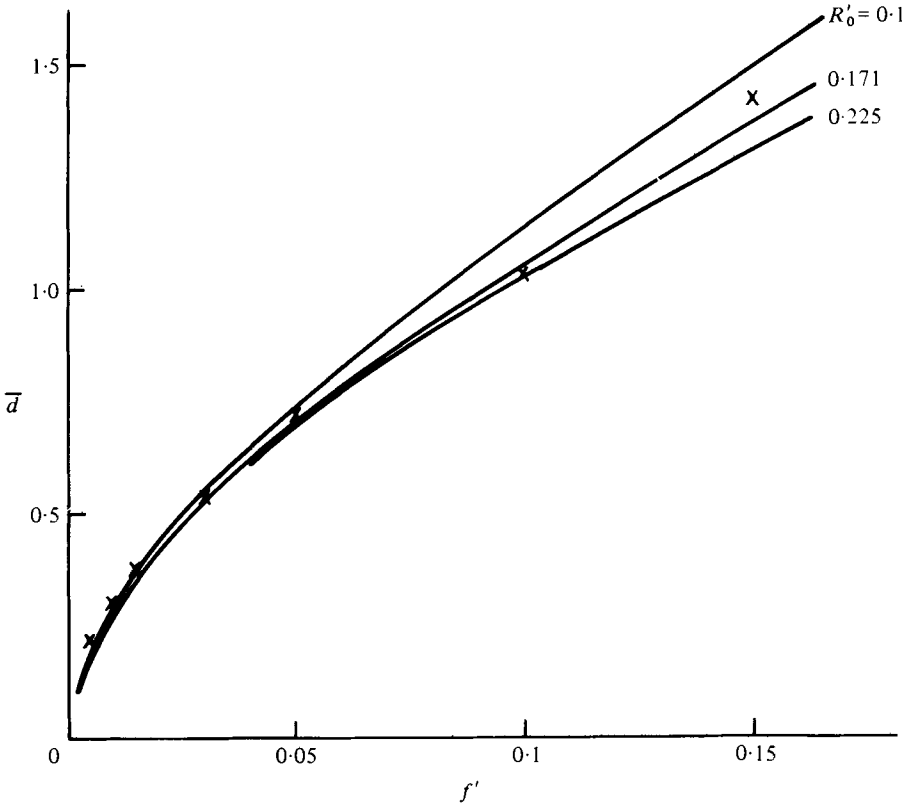

FIGURE 6. Graph of $\bar{d}(f', \bar{R}, \bar{R}'_0)$ for $\bar{R} = (\frac{1}{2})^{\frac{1}{2}}$, $\bar{R}'_0 = 0{\cdot}1$, $0{\cdot}171$, $0{\cdot}225$.
×, predicted values of $\bar{\delta}(f')$ with $\bar{R}'_0 = 0{\cdot}171$, and an appropriate $\bar{R}$ ($> \frac{1}{2}$).

where

$$e^2 = 4\bar{R}^2(4\bar{R}^2 + j^2\bar{d}^2)^{-1}. \tag{74}$$

Then, by substituting in (73) for G and H from (28) and (31),

$$\bar{U}_m = 2\bar{R}^{-1} \sum_{j=1}^{\infty} e(K(e) - E(e)). \tag{75}$$

We non-dimensionalize (70), and find that the solution $\bar{d}$ must satisfy

$$\bar{U}_s + 2\bar{R}^{-1}V(\bar{d}^2/4\bar{R}^2) = 2\bar{d}/\pi f' \tag{76}$$

as a function of $\bar{R}$ and $\bar{R}'_0$, hence of λ and $\bar{R}'_0$. The function V is defined as

$$V(\mu^2) = \sum_{j=1}^{\infty} e(K(e) - E(e)), \tag{77}$$

with

$$e^2 = (1 + j^2\mu^2)^{-1}.$$

The solution $\bar{d}$ to (76) depends slightly on $\bar{R}'_0$, but is not significantly affected when $\bar{R} = \lambda^{\frac{1}{2}}$ varies between $(\frac{1}{2})^{\frac{1}{2}}$ and 1. A graph of $\bar{d}(f')$ for $\bar{R} = (\frac{1}{2})^{\frac{1}{2}}$ and three values of $\bar{R}'_0$ is shown in figure 6, together with values of $\bar{\delta}(f')$ predicted by the model. There is good agreement between the results of the above calculations and the model's predictions, which gives confidence that the model converges to a realistic solution.

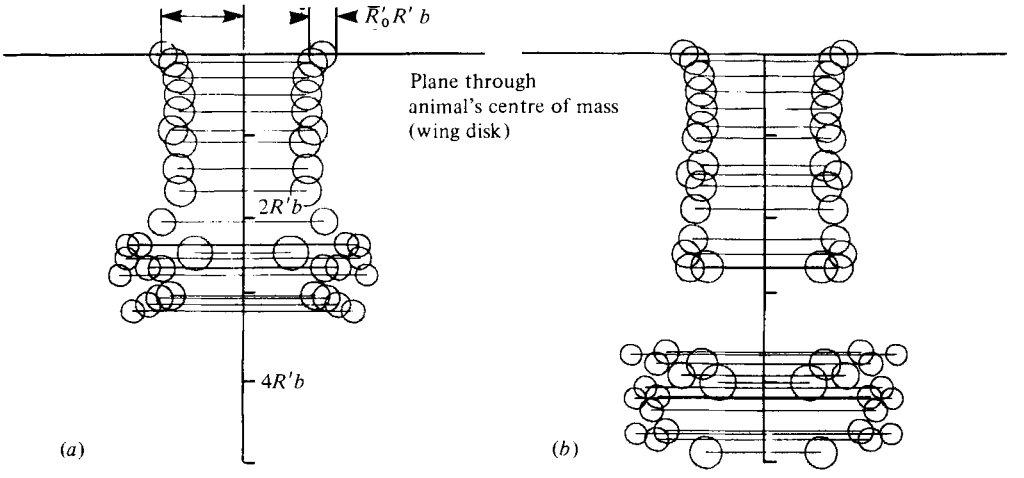

FIGURE 7. Diagrammatic cross-section through hovering vortex wake for a small insect (e.g. *Tipula* or *Eristalis*) ($f' = 0{\cdot}005$). Circles represent vortex cores; larger radius rings have smaller cores. Note smooth boundary of stack of rings just below the wing disk. At this (low) value of f' rings are close enough together for inflow through the boundary to be small, so that areal contraction is only slightly greater than one-half. In (*a*), 21 rings are present and a bound vortex is being formed at the lower end of the stack of rings. In (*b*), 29 rings are present and the bound vortex composed of the oldest 14 rings has broken away and no longer influences the flow. In figures 7–11 each vortex ring is drawn to scale; the initial core radius of each ring is $\bar{R}'_0R'b$.

6. Description of the wake

The observed structure of the wake depends largely upon the modified feathering parameter f' and the wing-disk vorticity specified by f_v. For large values of f' each ring has high circulation and travels fast; the spacing between the rings is large, therefore interaction between wake elements is small. There is no contraction, and the ring positions remain remarkably even all along the tube (figure 10).

For smaller values of f' the circulation of each ring is less, and interaction becomes more significant. A longer time is required for convergence to be achieved and there is also a limited amount of non-destructive instability in the far field. For very small f' adjoining rings approach closely, there is less opportunity for inflow through the wake boundary, and the solution approaches the vortex sheet associated with the momentum jet (see §2).

The more interesting results concern the range $f' \lesssim 0{\cdot}1$, and it is this range that we shall discuss in detail. As time proceeds the first vortex rings generated join to form what is effectively a single ring of large radius which travels at the open lower end of the wake. The general pattern is similar to that shown in figure 7 (*a*). If the analogy with the momentum jet were exact the succeeding rings would describe a smooth tube stretching back from the inner boundary of this bound ring to the wing disk and at some intermediate point reaching a minimum radius which would give the contraction coefficient we require. Around this minimum contraction the wake boundary should be cylindrical with constant spacing determined approximately by (76). This structure is indeed observed for very small values $f' < 10^{-3}$, too small to be realistic for flying animals; adjacent rings are close enough to overlap and the wake

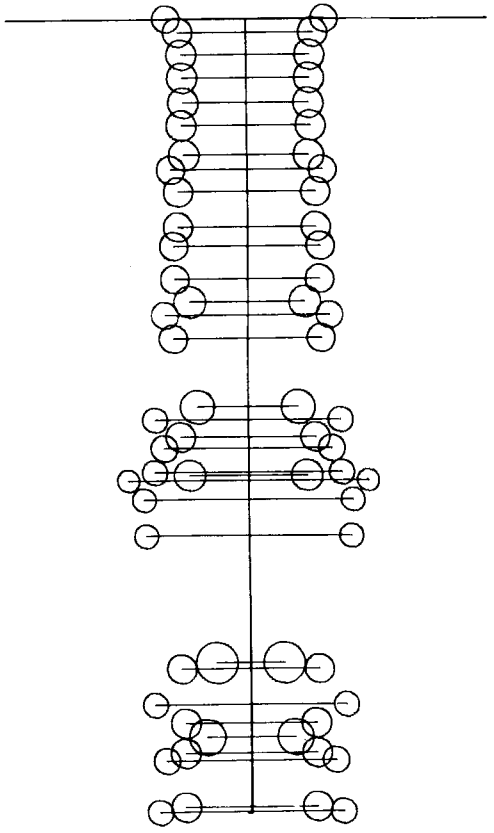

FIGURE 8. Wake for a moderate sized insect or hummingbird, showing breakup occurring after large time. $f' = 0{\cdot}01$, $\bar{R}_0' = 0{\cdot}171$.

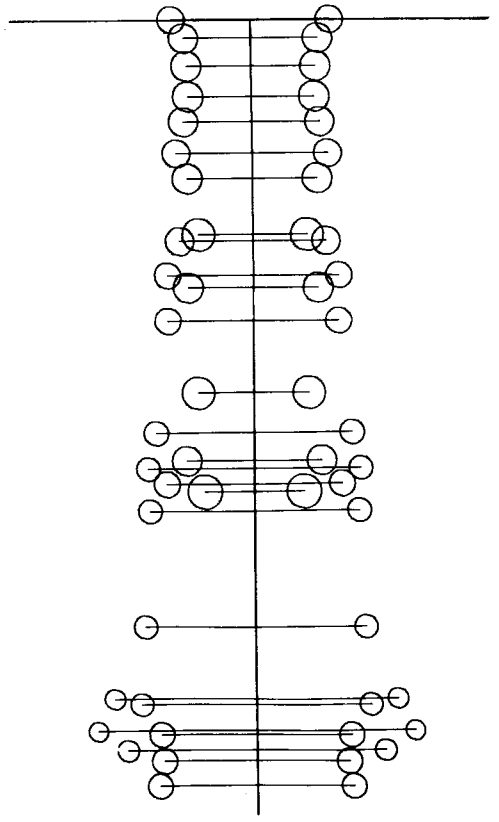

FIGURE 9. Wake for a large insect after 29 interations, showing a well-defined contraction neck and far-field break-up. $f' = 0{\cdot}015$, $\bar{R}_0' = 0{\cdot}171$.

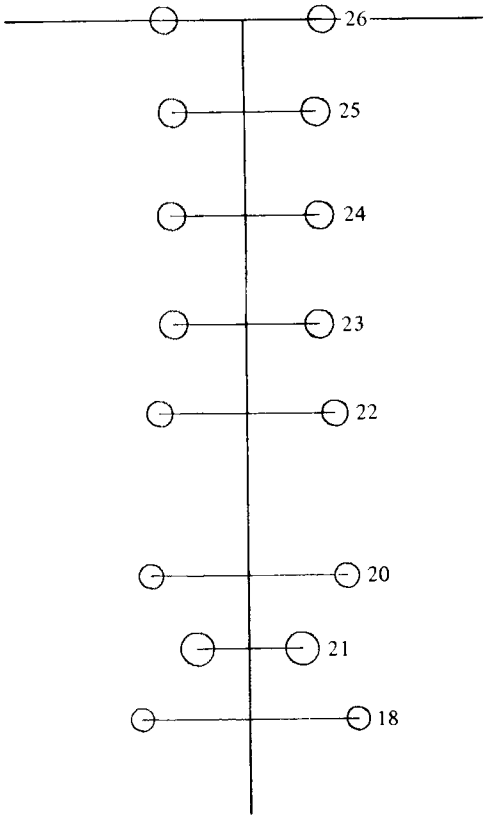

FIGURE 10. More stable wake for a large bird after 25 iterations. Rings are numbered consecutively; note that ring 21 has passed through ring 20, and that ring 19 has passed beyond the picture. $f' = 0{\cdot}15$, $\bar{R}_0' = 0{\cdot}171$.

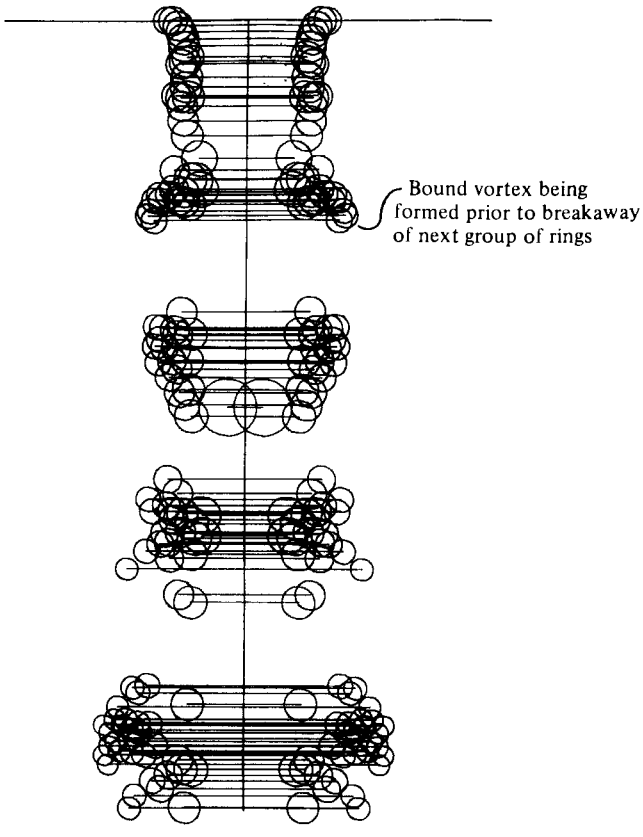

FIGURE 11. Wake for very small f', unrealistic for any animals, after 110 iterations. Note the clear bound vortex, and also far-field breakup, which appears to remain very stable. $f' = 10^{-3}$, $\bar{R}'_0 = 0{\cdot}171$.

boundary resembles the vortex sheet; not surprisingly, the smallest contraction coefficients are measured in this regime (figure 11).

With larger values of f', say $0{\cdot}005 \leqslant f' \leqslant 0{\cdot}015$, the spacing is also larger; in the contraction region the rings follow a smooth path, but are sufficiently far apart for entrainment into the wake to be possible under the influence of the starting ring; as a result larger contraction coefficients are observed. This range covers the majority of the insects; sample wake configurations are shown as figures 7–9. In all the diagrams of the wake the top ring – that most recently generated – lies on the wing disk, and has radius $R'b$. As we have seen in §5, R' depends on the wing circulation, but not on f. The ratio λ_0^2 is typically between $\frac{2}{3}$ and $\frac{5}{8}$, reaching 1 in the case of the Coleoptera; a reasonable wing circulation might give $R'^2/\lambda_0 = 0{\cdot}9$, whence $R' = 0{\cdot}8$ is a good estimate.

Figure 12 shows measured values for the contraction coefficient λ as a function of f for typical values of R', with $\bar{R}_0 = 0{\cdot}171$ and a semi-sine-squared f_v. Figures 7–11 show contraction occurring for different values of f'. Values of $\lambda'(f')$ are measured from plots such as these to within graphical accuracy; λ' is the contraction relative to the initial ring area $\pi R'^2 b^2$. Thus the far-field area is $\pi R'^2 b^2 \lambda'(f')$, which must equal $\pi b^2 \lambda(f)$, where λ is the true contraction coefficient relative to the wing-disk area.

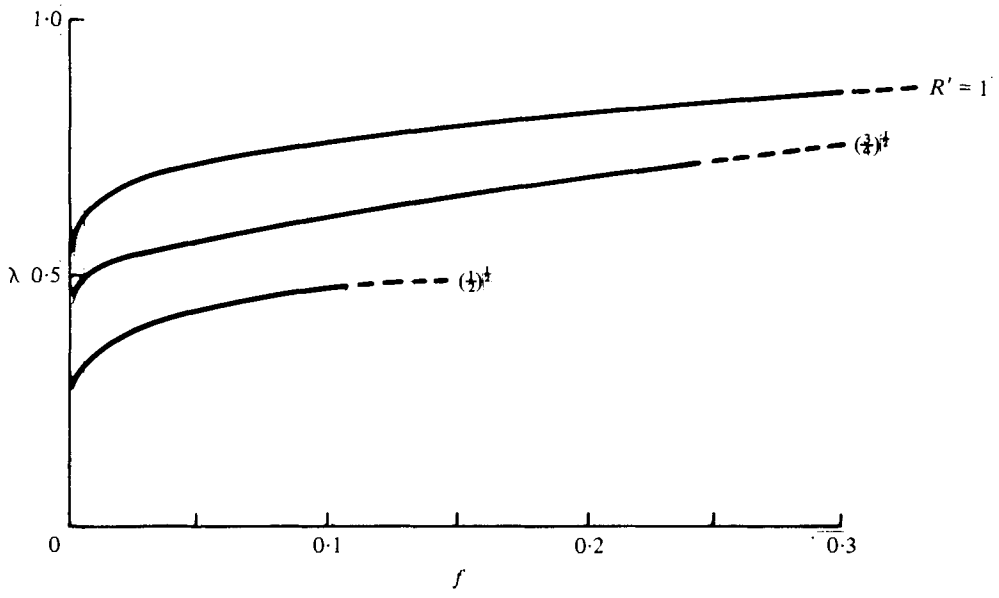

FIGURE 12. Graph of measured contraction coefficients λ relative to disk area as a function of f for various ring radii R', with $\bar{R}'_0 = 0{\cdot}171$, and a semi-sine-squared f_v. Dashed portions of curves indicate that rings expand in the far field, so that λ cannot be measured.

Therefore
$$\lambda(f) = R'^2\lambda'(f'). \tag{78}$$

In this way it is possible for λ to take values substantially smaller than the value of $\frac{1}{2}$ relative to the disk area predicted as the minimum by momentum jet theory. Once again, the details of the formation of a vortex ring on the wing disk are very important. For large f', greater than about 0·3, the rings in the far field do not contract, but begin to expand immediately. In some cases they will tend to a steady far-field radius, in others they will continue to expand as they travel; unless R' is substantially smaller than the estimate of 0·8, wake expansion is unlikely to be relevant since these values of f' are unrealistically large. Expansion is indicated in figure 12 by a dashed continuation of the $\lambda(f)$ curves.

The diagrams of the wake in figures 7–11, and the graph of $\lambda(f)$ in figure 12, are all concerned with the 'average' conditions of semi-sine-squared disk vorticity and an initial core radius $\bar{R}'_0 = 0{\cdot}171$. Variations of $\bar{R}'_0$ produce small changes in ring spacing (figure 6) but do not greatly alter the contraction coefficients (these are approximately 1% lower if $\bar{R}'_0 = 0{\cdot}225$, 1% greater if $\bar{R}'_0 = 0{\cdot}1$). Variations in the form of the disk vorticity f_v are more important when f' is large. As we should expect, the spacing $\bar{\delta}$ which depends almost entirely on local conditions in the near-field wake, is not affected, but the contraction coefficient λ does change, and with it the whole structure of the far field. Fortunately, the energy, which is the main object of this calculation, is unchanged, so that it is not necessary to consider the true form of f_v too deeply. The step-function f_v [form 2, (68)] reduces the effect of disk vorticity to a minimum; all of the influences on a ring during the early part of its life cause it to contract, and the smallest values of λ' are observed, approximately 8% less than those with the more realistic semi-sine-squared growth. A linear f_v [form 1, (67)] has a sizeable influence towards expansion during the early life of a ring; contraction coefficients

are much higher, and λ' becomes greater than 1 for $f' > 0{\cdot}1$. It is difficult to know how widely this form of f_v is relevant; although it may apply to some insects with unusual flight mechanisms (e.g. Lepidoptera, *Drosophila*), it is unlikely to apply to any animals for which f' is as large as 0·1. This is well into the size range of the birds, when a semi-sine-squared f_v is almost certainly appropriate.

Another aspect of the wake which becomes apparent after a number of wing-beats is its stability. Levy & Forsdyke (1927) have demonstrated that a chain of parallel vortex rings is unstable to radial and longitudinal perturbations for all spacing-to-radius ratios. Their calculations are purely infinitesimal and do not suggest how perturbations would grow. We find that instabilities do not grow indefinitely, but that adjacent rings join together to form separate larger vortex rings. This configuration is observed at all values of f' except very large values ($> 0{\cdot}1$), where adjacent rings are sufficiently far apart for interaction between them to be small. This instability does not occur within two radii of the wing disk, so that the contraction region will be unaffected by the perturbed velocity field. In figure 7(*a*), after 20 cycles a large vortex is clearly developing at the open end of the chain; in figure 7(*b*), 8 cycles later, this large vortex has broken away and a replacement is beginning to form, before the pattern repeats. Figure 11 shows the situation for a small value of f' ($= 0{\cdot}001$) after very large time; three large vortices each composed of about 25 individual rings are present, and a fourth is beginning to form. Once this structure has developed, the wake appears to be very stable, although for still larger times there may be some amalgamation of the larger rings. A similar, though less clearly defined, breakup is shown for larger values of f' in figures 8 and 9. In all cases the contraction region remains very stable, and self-consistent.

This controlled instability is not destructive, and appears to be less likely to destroy the character of the wake than viscous dissipation, which is not considered here. It does imply a periodicity which might be of physical relevance. There are a number of observations (C. P. Ellington, private communication) that hovering insects oscillate vertically at a frequency several times slower than their wing-beats; it is conceivable that the impulsive reaction of the wake instability is the cause. It is of course possible that body inertia is too great for this to be significant, and that the oscillation is caused by minor changes in stroke kinematics to assist position and direction sensing.

In figure 10, f' is large and there is no tendency for adjoining rings to coalesce, but some rings have passed through their neighbours, so that two adjacent rings have changed position. This effect was predicted by Kelvin, and was mentioned above (§4). Maxworthy's prediction of rings joining together is observed when f' is much smaller; rings are then much closer together, and the induced velocities from other rings in the chain have a significant effect.

It will be noted in figures 7, 8 and 11 that when f' is small ($\lesssim 0{\cdot}01$) adjoining rings overlap, and that for the very smallest f' the centre of a vortex core can often fall within the cores of adjacent rings. This small spacing is to be expected as the convection velocity is proportional to the circulation κ, which is itself proportional to f'. The wake is close to the momentum jet, and there can be little inflow through the wake boundary, so that the assumptions of mass and momentum conservation are valid. The measured contraction λ' in figure 11 ($f' = 0{\cdot}001$) is only slightly greater than $\frac{1}{2}$. The objection can be raised that the Biot–Savart formula for the induced

velocity of a vortex ring (20) approximates the ring by a line vortex, and that this formula is applied outside its range of validity. In fact, the method used to calculate the induced velocity [(20–(34)] is accurate quite close to the vortex core because the numerical routines used to calculate K and E are very accurate as e approaches unity (although of course the calculation of K breaks down when $e = 1$). It is unlikely that use of the three-dimensional form of the Biot–Savart law, with its attendant numerical difficulties, will give any more accurate results.

7. Energy consumption and induced power

The most important restriction on an animal's flight fitness is the amount of energy the chosen mode of flight consumes; there is a definite upper limit on the rate at which oxygen can be supplied to the muscles and converted into mechanical work. By allowing an oxygen debt to develop, a higher rate of working can be achieved for a limited period (as is probably the case for the flycatcher; Norberg 1975). Weis-Fogh & Alexander (1977) estimate the maximum mechanical power available from striated muscle operating continuously without an oxygen debt as about 250 W per kg muscle mass; birds are unlikely to achieve this power output.

The muscles must provide sufficient power to overcome the form and frictional drag (profile power) and the inertia of the wings (inertial power), and to generate the wake which supports the animal (induced power); in forward flight it is also necessary to overcome the form and frictional drag of the body but this is small in hovering. Weis-Fogh (1972, 1973) has discussed the methods by which profile and inertial powers are calculated, but calculates profile and induced power together by the use of general drag coefficients and measured wing polars; this method introduces all of the uncertainty of lift and drag coefficients and the steady-state assumptions. The method suggested here is to calculate profile and inertial power according to the method of Weis-Fogh (q.v.); the drag coefficient to be used for the profile power is that at zero lift; for *Drosophila* $C_D \approx 0{\cdot}35$ (Vogel 1967), for the hummingbird *Amazilia* $C_D \approx 0{\cdot}04$ (Weis-Fogh 1972), and a good estimate for birds in general is $C_D \approx 0{\cdot}02$. In hovering flight of birds both the profile and the inertial power calculated in this way are negligible compared with the induced power and can be neglected. For the insects they form a substantial part of the total power and cannot be ignored.

We are concerned here with the induced power P_i, calculated by the method of §4, (40)–(55), for the wake configuration specified by the iterative procedure (58). Since the induced power $P_{i,M}$ for the momentum jet is an estimate of the true induced power, P_i is expressed as the ratio σ to the momentum-jet value given by (53) and (55). As the momentum jet is an ideal description of the wake corresponding to the minimum energy state we should not expect σ to take values less than 1. Where it does so is probably the result of numerical inaccuracies; it never takes values less than 0·93.

A graph of σ against f for various values of R' and $\bar{R}'_0$ is shown in figure 13. For the insects ($0{\cdot}005 < f < 0{\cdot}015$), σ is close to 1, the exact value depending on R' and to a lesser extent $\bar{R}'_0$; it is given approximately by $\sigma = 1/R'$; variations with f are small. Thus a simple correction factor to the momentum-jet induced power is adequate. Therefore for the insects, with an accuracy of $\pm 5\%$,

$$P_i = \frac{Mg}{R'}\left(\frac{Mg}{2\rho A}\right)^{\frac{1}{2}} = P'_{i,M}. \tag{79}$$

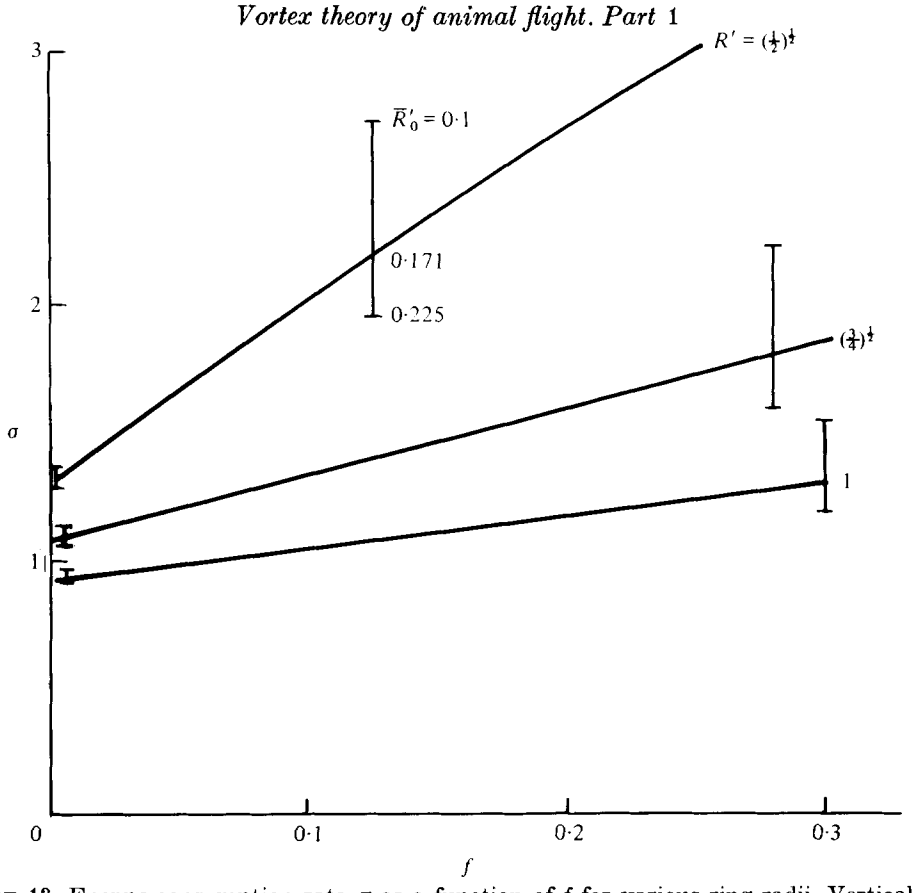

FIGURE 13. Energy consumption rate σ as a function of f for various ring radii. Vertical bars show tolerance to variations in core radius $\bar{R}'_0$; tolerance to disk vorticity is negligible and is not shown. Note that the $\sigma(f)$ curves are very close to straight lines.

This is the induced power required for a momentum jet generated by an actuator disk of radius $R'b$; as has been stated above, in this range of f the momentum-jet and vortex-ring wakes are close provided that the actuator disk is correctly defined. We may conclude that for insects the momentum jet is a good description of the flow, and predicts power consumption accurately. The vortex-ring model displays the formation of a large ring at the lower end of the chain of rings, and also some controlled instability.

For the birds, the momentum-jet power $P_{i,M}$ [or even the modified momentum-jet power $P'_{i,M}$, defined in (79)] greatly underestimate the true power. Indeed, σ increases almost linearly with f, according to the approximate formula

$$\sigma = \frac{0{\cdot}95}{R'} + \frac{1{\cdot}2}{R'^5} f, \tag{80}$$

from the graph of figure 13, when $\bar{R}'_0 = 0{\cdot}171$; similar formulae can be found for other values of $\bar{R}'_0$. This formula permits a rapid estimate of the induced hovering power for any bird provided that f and R' are known.

Calculations showing the application of the above results to several species are given in Rayner (1979*b*, §2). These indicate the range of adaptive measures taken to reduce the energy cost of hovering flight.

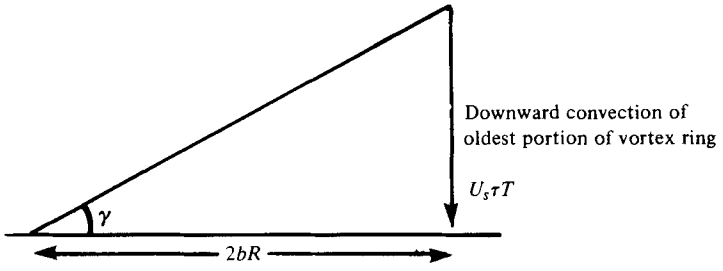

FIGURE 14. Notation for calculation of stroke-plane angle γ in hovering flight.

The most important conclusion from this work is the excess induced power in avian hovering due to the separation of vortex rings in the wake. This implies that birds (other than hummingbirds, for which f is small) experience considerable difficulty in meeting the power demands of sustained hovering, since the tip losses predicted by (80) are significant.

As an example, for the flycatcher, $f = 0{\cdot}044$; with a R' of 0·67, $\sigma = 1{\cdot}81$, so that the animal requires 0·23 W to hover continuously. The major pectoral muscles, which are of mass $1{\cdot}9 \times 10^{-3}$ kg, working continuously at optimum efficiency would produce a maximum of $1{\cdot}9 \times 10^{-3} \times 250 = 0{\cdot}48$ W according to Weis-Fogh's estimates. Since they operate for only about one-half of the total wing-beat, a more realistic maximum is about 0·20 W; thus, if the flycatcher were hovering aerobically, it would be at the very limit of its possible range, and hovering is more likely to be anaerobic at a lower efficiency, especially so if R' is as low as 0·67. At this value of σ the tip losses are as high as 17% of the total induced power, compared with $P'_{i,M}$.

The above calculation is purely an example of how the rule-of-thumb expression (80) can be used to estimate the hovering fitness of birds; for a more exact calculation profile and inertial power must be included. Knowledge of the chemical efficiency of the muscles will indicate whether such hovering is possible aerobically or anaerobically.

8. Inclination of the stroke plane

We have already seen that the stroke plane must be inclined to the horizontal so that the net wake momentum is vertical; as a feature of this model we assume that *all* vortex elements have vertical momentum. We perform a simple calculation to estimate the angle γ at which the stroke plane is tilted, for comparison with observations. The notation used is in figure 14.

Neglecting the effect of other vorticity present in the wake, the starting vortex will travel down under its self-induced velocity, which is approximately that of a single element of the chain, U_s, which is given by (17) with $R = R'b$ and $R_0 = \bar{R}'_0 R'b$. Therefore, if $\bar{A} = \frac{1}{4}$,

$$\tan\gamma = U_s \tau T / 2bR' \tag{81}$$

$$= \tfrac{1}{4}\pi \frac{\tau T}{T_w} \frac{f}{R'^4} \left(\log_e \frac{8}{\bar{R}'_0} - \tfrac{1}{4} \right). \tag{82}$$

For the birds we have $\tau \approx \frac{3}{7}$ and $T_w = T$, while for the insects and hummingbirds

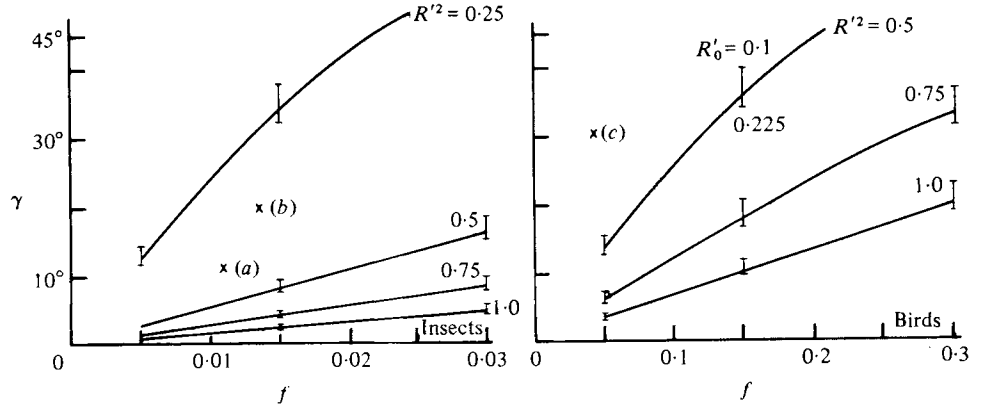

FIGURE 15. Stroke-plane angle γ as a function of f for insects and birds, with core radius $\bar{R}'_0 = 0{\cdot}171$. Vertical bars indicate tolerance to variations in $\bar{R}'_0$. This figure also indicates observations: (*a*) *Amazilia* (Weis-Fogh 1972); (*b*) *Drosophila* (Weis-Fogh 1972); (*c*) *Ficedula hypoleuca* (Norberg 1975).

we have $\tau = \frac{1}{2}$ and $T_w = \frac{1}{2}T$. Of course, this calculation involves a good deal of approximation, and it is difficult to be certain of its accuracy. In particular, U_s is likely to be about 25% too low as the effect of the rest of the wake is not included.

Calculated values of γ for birds and insects are shown in figure 15, together with some observations. The effect of varying R' is important while that of varying $\bar{R}'_0$ is small, and negligible for the insects. The observations seem to suggest a much larger value of R' than is consistent with energy saving, for an R' as small as 0·6 would imply a significant increase in power consumption and it is unlikely that wing aerodynamics would dictate such an inefficient circulation distribution. The error more probably lies in the underestimate of U_s in the calculation above. Nevertheless, predicted stroke-plane angles agree with what we might expect; this calculation moreover ignores any physiological constraints. It is valid both for the downstroke of a hovering bird or for either branch of the figure of eight of a hovering insect.

9. Conclusions

(i) A hovering animal's wing-beat generates a vortex ring which may perhaps be modelled efficiently as a circular ring.

(ii) A good model of the hovering wake is then a chain of stacked vortex rings for both birds and insects.

(iii) The structure of the wake is developed as it starts from rest. Despite some breakup and limited instability the solution indicates clearly the nature of a consistent wake configuration.

(iv) The entire wake system is described by three parameters: the feathering parameter f, whose range is $0{\cdot}005 \leqslant f \leqslant 0{\cdot}015$ for insects and $0{\cdot}05 \leqslant f \leqslant 0{\cdot}15$ for birds; the initial ring radius R'; the initial ring core radius $\bar{R}'_0$.

R' and $\bar{R}'_0$ (of which the latter generally has only a minor influence) are determined by the initial energy and impulse of a vortex ring. A useful parameter is the modified feathering parameter $f' = f/R'^4$.

(v) For small f' and large times the wake becomes close to the momentum jet.

(vi) The contraction coefficient increases with f' because of recirculation in the contraction region and the lack of strict conservation of mass and momentum within the wake region. For large values of f' the wake expands.

(vii) The spacing between adjacent rings measured in the contraction region is very close to that for a consistent family of identical parallel rings.

(viii) Periodic breakup of the wake is observed for smaller values of f', though the instability is limited to the far field and is not destructive. This may be an alternative explanation for the low frequency oscillations of insects in a vertical plane when hovering, which are usually ascribed to position finding.

(ix) The power required to hover has been calculated. The values obtained may be related by a conversion factor of simple form to the momentum jet power. For the insects this factor depends solely on R', for the birds on both f and R'.

(x) The values found for the initial vortex-ring radius R' are all less than 1, and depend on the wing circulation. An appropriate circulation distribution for both normal and avian hovering is proportional to radius times wing chord. For a bird this would give $R' \approx 0{\cdot}75$ (or perhaps less), for an insect with semi-elliptic wing $R' \approx 0{\cdot}85$.

(xi) The momentum jet generated by an actuator disk of area R'^2 times the wing-disk area is a good description of the wake of a hovering insect. It estimates the induced power accurately, but does not predict the presence of a large ring at the open lower end of the vortex wake. For the birds the feathering parameter is much larger, and the momentum jet cannot be an adequate description of the wake.

(xii) Tip losses in hovering flight, calculated as the difference between the induced power and modified momentum-jet-induced power, can be as high as 15–20% in avian hovering, but are negligible in normal hovering.

(xiii) The experimental observations by Magnan *et al.* and by Ellington show vortex rings similar to those used in this model. Further observations of this kind will provide much useful information on the nature of the flow field and will assist the verification of the hypotheses put forward in this paper. Calculations of the expected stroke-plane angle are in general agreement with observations.

The author would like to thank all those who have offered help and advice during the course of this work, in particular Professor Sir James Lighthill, C. P. Ellington, Dr K. E. Machin and Dr T. J. Pedley, and also acknowledges the financial assistance of the Science Research Council.

REFERENCES

Batchelor, G. K. 1967 *An Introduction to Fluid Dynamics.* Cambridge University Press.

Cone, C. D. 1968 The aerodynamics of flapping birdflight. *Spec. Sci. Rep. Va Inst. Mar. Sci.* no. 52.

Ellington, C. P. 1978 The aerodynamics of normal hovering flight. In *Comparative Physiology – Water, Ions and Fluid Mechanics* (ed. K. Schmidt-Nielsen, L. Bolis & S. H. P. Maddrell), pp. 327–345. Cambridge University Press.

Fraenkel, L. E. 1970 On steady vortex rings of small cross-section in an ideal fluid. *Proc. Roy. Soc.* A **316**, 29–62.

GLAUERT, H. 1935 Airplane propellors. In *Aerodynamic Theory* (ed. W. H. Durand), vol. 4, pp. 169–360. Springer.

GRADSHTEYN, I. S. & RHYZHIK, I. M. 1965 *Tables of Integrals, Series and Products*. Academic Press.

GREENEWALT, C. H. 1962 Dimensional relationships for flying animals. *Smithson. Misc. Collns* **144**, 2.

HAINSWORTH, F. R. & WOLF, J. L. 1972 Power for hovering flight in relation to body size in hummingbirds. *Am. Nat.* **106**, 589–596.

HOFF, W. 1919 Der Flug der Insekten. *Naturwissenschaften* **7**, 159–164.

KÁRMÁN, T. VON & BURGERS, J. M. 1935 General aerodynamic theory – perfect fluids. In *Aerodynamic theory* (ed. W. H. Durand), vol. 2, pp. 315–352. Springer.

LAMB, H. 1932 *Hydrodynamics*. Cambridge University Press.

LEVY, H. & FORSDYKE, A. G. 1927 The stability of an infinite system of circular vortices. I. *Proc. Roy. Soc.* A **114**, 594–604.

LIGHTHILL, M. J. 1973 On the Weis-Fogh mechanism of lift generation. *J. Fluid Mech.* **60**, 1–17.

LIGHTHILL, M. J. 1977 Introduction to the scaling of aerial locomotion. In *Scale Effects in Animal Locomotion* (ed. T. J. Pedley), pp. 365–404. Academic Press.

MAGNAN, A., PERRILLIAT-BOTONET, C. & GIRARD, H. 1938 Essais d'enregistrements cinématographiques simultanées dans trois directions perpendiculaires deux à deux de l'écoulement de l'air autour d'un oiseau en vol. *C. R. hebd. Séanc. Acad. Sci., Paris* **206**, 462–464.

MAXWORTHY, T. 1972 The structure and stability of vortex rings. *J. Fluid Mech.* **51**, 15–32.

MAXWORTHY, T. 1977 Some experimental studies of vortex rings. *J. Fluid Mech.* **81**, 465–495.

NACHTIGALL, W. 1974 *Insects in Flight*. London: George Allen & Unwin.

NACHTIGALL, W. & KEMPF, B. 1971 Vergleichende Untersuchungen zur flugbiologischen Funktion des Daumenfittichs (*Alula spuria*) bei Vögeln. *Z. vergl. Physiol.* **71**, 326–341.

NORBERG, U. M. 1975 Hovering flight in the pied flycatcher (*Ficedula hypoleuca*). In *Swimming and Flying in Nature* (ed. T. Y. Wu, C. J. Brokaw & C. Brennen), vol. 2, pp. 869–881. Plenum.

NORBERG, U. M. 1976 Aerodynamics of hovering flight in the long-eared bat *Plecotus auritus*. *J. Exp. Biol.* **65**, 459–470.

NORBURY, J. 1973 A family of steady vortex rings. *J. Fluid Mech.* **57**, 417–431.

OEHME, H. & KITZLER, U. 1974 Untersuchungen zur Flugbiophysik und Flugphysiologie der Vögel. I. Über die Kinematik des Flügelschlages beim unbeschleunigten Horizontalflug. *Zool. Jb. Physiol.* **78**, 461–512.

OEHME, H. & KITZLER, U. 1975*a* Untersuchungen zur Flugbiophysik und Flugphysiologie der Vögel. II. Zur Geometrie des Vögelflügels. *Zool. Jb. Physiol.* **79**, 402–424.

OEHME, H. & KITZLER, U. 1975*b* Untersuchungen zur Flugbiophysik und Flugphysiologie der Vögel. III. Die Bestimmung der Muskelleistung beim Kraftflug der Vögel aus kinematischen und morphologischen Daten. *Zool. Jb. Physiol.* **79**, 425–458.

OSBORNE, M. F. M. 1951 Aerodynamics of flapping flight with applications to insects. *J. Exp. Biol.* **28**, 221–245.

PENNYCUICK, C. J. 1968 Power requirements for horizontal flight in the pigeon *Columba livia*. *J. Exp. Biol.* **49**, 527–555.

RAYNER, J. M. V. 1979*a* A vortex theory of animal flight. Part 2. The forward flight of birds. *J. Fluid Mech.* **91**, 739–771.

RAYNER, J. M. V. 1979*b* A new theory of animal flight mechanics. *J. Exp. Biol.* (In the Press.)

RÜPPELL, G. 1977 *Bird Flight*. Van Nostrand–Rheinhold.

SAFFMAN, P. G. 1970 The velocity of viscous vortex rings. *SIAM J.* **49**, 371–380.

VOGEL, S. 1967 Flight in *Drosophila*. III. Aerodynamic characteristics of fly wings and wing models. *J. Exp. Biol.* **46**, 431–443.

WEIS-FOGH, T. 1972 Energetics of hovering flight in hummingbirds and *Drosophila*. *J. Exp. Biol.* **56**, 79–104.

WEIS-FOGH, T. 1973 Quick estimates of flight fitness in hovering animals, including novel mechanisms for lift production. *J. Exp. Biol.* **59**, 169–230.

WEIS-FOGH, T. 1977 Dimensional analysis of hovering flight. In *Scale Effects in Animal Locomotion* (ed. T. J. Pedley), pp. 405–420. Academic Press.

WEIS-FOGH, T. & ALEXANDER, R. MCN. 1977 The sustained power output from striated muscle. In *Scale Effects in Animal Locomotion* (ed. T. J. Pedley), pp. 511–525. Academic Press.

WIDNALL, S. E. & SULLIVAN, J. P. 1973 On the stability of vortex rings. *Proc. Roy. Soc.* A **332**, 335–353.

WIDNALL, S. E. & TSAI, C.-Y. 1977 The instability of the thin vortex ring of constant vorticity. *Phil. Trans. Roy. Soc.* A **287**, 273–305.